NASA/TM-2008-215339
NESC-RP-08-09/06-081-E

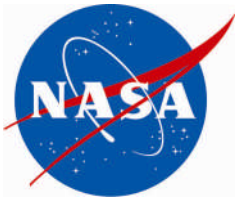

Ares I-X Upper Stage Simulator Residual Stress Analysis

Ivatury S. Raju
NASA Langley Research Center, Hampton, Virginia

Frederick W. Brust
Engineering Mechanics Corporation of Columbus, Columbus, Ohio

Dawn R. Phillips
Lockheed Martin Mission Services, Hampton, Virginia

Derrick Cheston
NASA Glenn Research Center, Cleveland, Ohio

August 2008

The NASA STI Program Office . . . in Profile

Since its founding, NASA has been dedicated to the advancement of aeronautics and space science. The NASA Scientific and Technical Information (STI) Program Office plays a key part in helping NASA maintain this important role.

The NASA STI Program Office is operated by Langley Research Center, the lead center for NASA's scientific and technical information. The NASA STI Program Office provides access to the NASA STI Database, the largest collection of aeronautical and space science STI in the world. The Program Office is also NASA's institutional mechanism for disseminating the results of its research and development activities. These results are published by NASA in the NASA STI Report Series, which includes the following report types:

- TECHNICAL PUBLICATION. Reports of completed research or a major significant phase of research that present the results of NASA programs and include extensive data or theoretical analysis. Includes compilations of significant scientific and technical data and information deemed to be of continuing reference value. NASA counterpart of peer-reviewed formal professional papers, but having less stringent limitations on manuscript length and extent of graphic presentations.

- TECHNICAL MEMORANDUM. Scientific and technical findings that are preliminary or of specialized interest, e.g., quick release reports, working papers, and bibliographies that contain minimal annotation. Does not contain extensive analysis.

- CONTRACTOR REPORT. Scientific and technical findings by NASA-sponsored contractors and grantees.

- CONFERENCE PUBLICATION. Collected papers from scientific and technical conferences, symposia, seminars, or other meetings sponsored or co-sponsored by NASA.

- SPECIAL PUBLICATION. Scientific, technical, or historical information from NASA programs, projects, and missions, often concerned with subjects having substantial public interest.

- TECHNICAL TRANSLATION. English-language translations of foreign scientific and technical material pertinent to NASA's mission.

Specialized services that complement the STI Program Office's diverse offerings include creating custom thesauri, building customized databases, organizing and publishing research results ... even providing videos.

For more information about the NASA STI Program Office, see the following:

- Access the NASA STI Program Home Page at ***http://www.sti.nasa.gov***

- E-mail your question via the Internet to help@sti.nasa.gov

- Fax your question to the NASA STI Help Desk at (301) 621-0134

- Phone the NASA STI Help Desk at (301) 621-0390

- Write to:
  NASA STI Help Desk
  NASA Center for AeroSpace Information
  7115 Standard Drive
  Hanover, MD 21076-1320

NASA/TM-2008-215339
NESC-RP-08-09/06-081-E

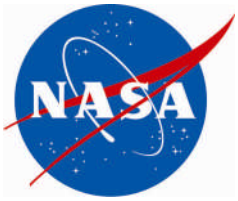

Ares I-X Upper Stage Simulator Residual Stress Analysis

Ivatury S. Raju
NASA Langley Research Center, Hampton, Virginia

Frederick W. Brust
Engineering Mechanics Corporation of Columbus, Columbus, Ohio

Dawn R. Phillips
Lockheed Martin Mission Services, Hampton, Virginia

Derrick Cheston
NASA Glenn Research Center, Cleveland, Ohio

NASA Engineering and Safety Center
Langley Research Center
Hampton, Virginia 23681-2199

August 2008

Available from:
NASA Center for AeroSpace Information (CASI)
7115 Standard Drive
Hanover, MD 21076-1320
(301) 621-0390

Ares I-X Upper Stage Simulator Residual Stress Analysis

Frederick W. Brust, Jr.
Engineering Mechanics Corporation of Columbus
Columbus, OH

Dawn R. Phillips
Lockheed Martin Mission Services
Hampton, VA

Ivatury S. Raju
NASA Langley Research Center
Hampton, VA

Derrick Cheston
NASA Glenn Research Center
Cleveland, OH

Abstract

The structural analyses described in the present report were performed in support of the NASA Engineering and Safety Center (NESC) Critical Initial Flaw Size (CIFS) assessment for the Ares I-X Upper Stage Simulator (USS) common shell segment. An independent assessment was conducted to determine the critical initial flaw size (CIFS) for the flange-to-skin weld in the Ares I-X Upper Stage Simulator (USS). The Ares system of space launch vehicles is the US National Aeronautics and Space Administration's plan for replacement of the aging space shuttle. The new Ares space launch system is somewhat of a combination of the space shuttle system and the Saturn launch vehicles used prior to the shuttle. Here, a series of weld analyses are performed to determine the residual stresses in a critical region of the USS. Weld residual stresses both increase constraint and mean stress thereby having an important effect on fatigue and fracture life. The results of this effort served as one of the critical load inputs required to perform a critical initial flaw size (CIFS) assessment of the same segment.

Table of Contents

Executive Summary

This report describes the weld residual stress analyses performed supporting the NESC Critical Initial Flaw Size (CIFS) assessment of the Ares I-X USS common tuna-can segments. Here, a series of weld analyses are performed to determine the residual stresses in a critical region of the USS. Weld residual stresses both increase constraint and mean stress thereby having an important effect on fatigue and fracture life. The results of this effort served as one of the critical load inputs required to perform a critical initial flaw size (CIFS) assessment of the same segment.

Computational weld modeling is challenging because many of the processes of welding are highly nonlinear. Material melts and re-solidifies, very high transient thermal gradients are experienced, non-linear temperature dependent plastic straining and phase transformations can occur, among other sources of nonlinearity. A well validated computational weld modeling code, Virtual Fabrication Technology (VFT^{TM}), was used here to predict the flange to shell weld residual stresses. There was not direct validation of the model predictions for the flange to shell weld discussed here. However, extensive validation of the computational weld model is available in the main body of the report for weld temperature predictions versus time, distortion predictions, and weld residual stresses so that predictions are presented here with confidence in their accuracy.

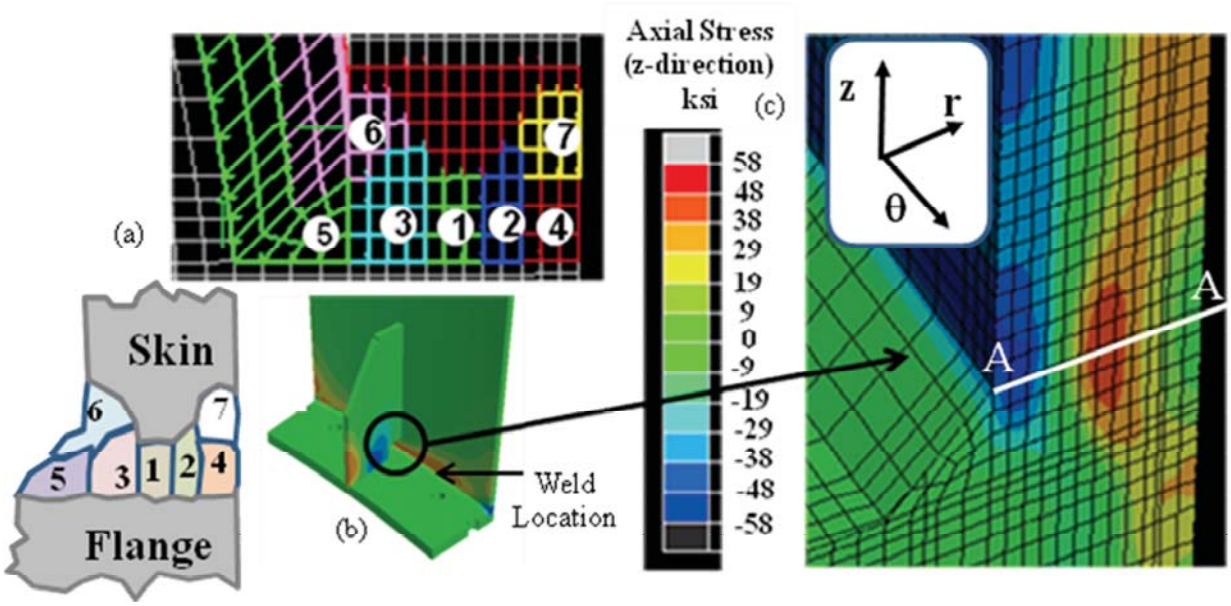

Figure ES- 1 Finite element weld model. (a) local finite element weld mesh showing 7 passes along with the definition of skin, flange, and passes (lower left insert), (b) weld residual stress location at stiffener 'mouse hole', (c) axial weld residual stress contour plot at 'mouse hole' location.

A large number of weld sequences, weld parameters, and weld geometries were investigated. Each weld pass is modeled by using a moving heat source as the weld is deposited. A ten-degree segment was modeled with appropriate boundary conditions.

The final sequence suggested by the NESC team is shown in Figure ES-1(a). It is seen that a 7 pass balanced weld sequence with **the final pass deposited on the OD is the optimum** since it induces compressive axial residual stresses on the ID at the toe of the weld (above). The location at the toe of the fillet at the mouse-hole location (Figure ES-1(b)) was determined to be the critical CIFS location. Circumferential cracks, driven by axial stresses are the controlling crack growth situation here since they combine unfavorably with service loads (Figure ES-1(c)).

The line plot in Figure ES-2 illustrates the axial residual stress patterns through the shell wall at the toe of the fillet that was used for the CIFS analysis. The plot location is at the toe of the fillet, plotted from the ID to OD at point 'A' in the Figure ES-2 right insert. The results with the final pass applied to the ID, which reverses passes 6 and 7 in the upper left inset (above), shows high tensile ID stresses. These stresses were conservatively used in the CIFS analysis even though an analysis shows that 'shakedown' occurs after the application of the first service load. Shakedown reduces the stresses in the line plot below.

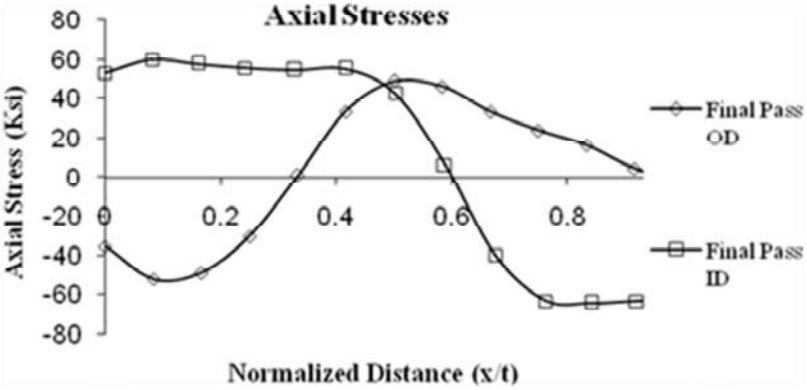

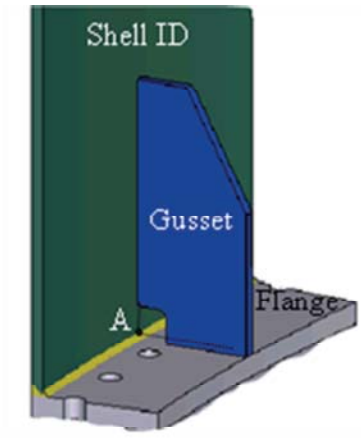

Figure ES- 2 Axial stress plot through shell wall (from ID to OD) at point 'A' at toe of the fillet weld under the gusset 'mouse hole'. This is the critical location for the CIFS assessment.

The residual stresses are strongly affected by pass sequence. The mechanism for this behavior is discussed in the main report body with many more details. The final weld residual stress pattern for the Ares shell to flange weld is the result of the competition between axial shrinkage of the weld bead, which produces tension at the final weld location, and radial shrinkage of the bead, which tends to produce tension on the ID and compression on the OD (analogous to shrink fitting a ring on a tube). The thick stiff ring and the gusset stiffener also complicate the final residual stress patterns.

Introduction

The Ares I-X Upper Stage Simulator (USS) is a mass simulator element for the Ares I system (see Figure 1). The USS is comprised of seven similar cylindrical shell segments, referred to as "tuna-can segments", and interface structures. Several tuna-can segments are identical in their design and are referred to as the common segments. Each tuna-can segment, as also shown in Figure 1 to the right, has a flange welded to each end allowing the different segments to be bolted together. The NASA safety standard for human spaceflight requires that critical structural components be designed so that the largest crack that can be missed by the appropriate NDE technique does not grow to a critical length within four lifetimes. Fracture mechanics must be used to analytically determine the maximum initial crack or flaw size that would not produce a critical stress intensity factor in the location of concern after four simulated life cycles. This critical initial flaw size is referred to as the CIFS. This report describes one contributor to the CIFS study – the residual stresses caused by the weld process.

The Ares I-X (AIX) Upper Stage Simulator (USS) represents the upper stage of the Ares I vehicle in mass, center-of-gravity, and outer mold line. To achieve a low manufacturing cost, the AIX inert upper stage is designed in a modular fashion consisting of cylindrical segments that are made of construction grade A516 Grade 70 plate steel with machined flanges welded onto either end for bolting adjacent segments. Keep in mind that this assessment is being made for the simulator only and will not be the flight material.

The flange-to-skin or flange-to-shell weld is one of several weld joints used in the design of the USS. The flange-to-skin weld is located at the outermost diameter of the upper stage simulator and is in the primary load path of the flight test vehicle (Figure 1). The USS consists of several "tuna can" segments that are approximately 5.5 m in diameter, 2.9 m tall, and 12.7 mm thick. A 152 mm wide by 25.4 mm thick flange is welded to the skin and is used to fasten adjacent tuna cans. Gussets are welded to the skin and flange every 10 degrees around the circumference of the "tuna can". The flange-to-skin weld is a flux core butt weld with a fillet weld on the inside surface. The welding process often creates loss of fusion defects in the weld that could develop into fatigue cracks and jeopardize the structural integrity of the Ares I-X vehicle.

A CIFS assessment was made for the welds within the common segments designated US-1 through US-7 whose shell and flange designs were identical. The US-1/US-2 interface flange-to-skin welds were chosen for the analysis because they experience the highest service loads. This weld represents a rather unique geometry, which cannot be modeled using an axis-symmetric model. Moreover, the geometry is quite different from typical 'pipe or cylinder' type welds and the results are not necessarily intuitive.

In this report the main features of the weld analysis are discussed and a brief summary of the CIFS assessment is provided. The purpose of this set of weld analyses is to model the weld process using a variety of sequences to determine the 'best' sequence in terms of

weld residual stresses and distortions. The many factors examined in this study include weld design (single-vee, double-vee groove), weld sequence, boundary conditions, and material properties, among others. In addition, mesh refinement studies are included. Full three dimensional weld analyses are performed. The results of this weld analysis are included with service loads (including fit-up stresses) to perform a fatigue and critical initial flaw size evaluation.

Weld Analysis Procedure

Computational weld modeling is challenging because many of the processes of welding are highly nonlinear. Material melts and re-solidifies, very high transient thermal gradients are experienced, non-linear temperature dependent plastic straining and phase transformations can occur, among other sources of nonlinearity. Moreover, for weld modeling to have practical advantages in industrial production, computational solution times must be manageable since an optimum weld design of large, complex fabrications requires numerous separate analyses. The many benefits of computational weld modeling are illustrated schematically in Figure 2. Control of weld residual stresses can lead to increased fatigue life, corrosion control, and improved fracture response. Distortion control can lead to reduced fabrication costs and improve fit-up and additional stresses caused by fit-up modifications. The final advantage for weld modeling illustrated in Figure 2 is microstructure control, including hardness. All of these can be modeled within the computational weld code used here.

Most computational weld models that are available commercially are mathematics and physics based models. The following is a brief description of the VFT^{TM} (Virtual Fabrication Technology, (Reference [1]) code which was used for the work reported here. Other codes are also available for predicting and controlling weld residual stresses and distortions. As illustrated in Figure 3, there are three main analysis modules, the graphical user interface (used to define weld passes, set up the model and material properties, etc.), the thermal model and the structural model, that make up the weld process simulation methodology in VFT that are briefly summarized below. Welding distortion simulation normally adopts sequentially coupled thermal structural analysis. First, the thermal analysis is performed. Then the structural analysis is performed using the temperatures predicted by the thermal analysis as the thermal load in conjunction with any additional mechanical loads or constraints. Material response in a welding process is very much localized along the welds. For large fabricated structures, the simulations involve millions of degrees of freedom and are highly nonlinear, and hence are extremely computationally intensive. As such, coarse meshes must be used for the global distortion predictions. However, numerical thermal predictions using such coarse meshes are inadequate, especially for capturing the thermal gradients and cooling rates during welding processes. Developing efficient and effective simulation procedures that take into account these contrasting requirements is crucial to practically and successfully applying welding simulations to large problems.

Thermal Solutions and CTSP

The thermal model (CTSP) was developed based on superposition of complicated closed form analytical expressions and developed heat source theories. CTSP is very rapid and

is used for large problems. Numerical thermal solutions based on a modification of Goldak theory [8] are also used, but these solutions often take a long time to perform for large problems. The CTSP solutions were used here because they have been shown to be very accurate for large problems and solution times are on the order of several minutes compared with hours and days for a full numerical thermal solution.

Comprehensive Thermal Solution Procedure (CTSP) [4, 5, 8-10] is a closed form solution thermal analysis code specifically developed for global distortion and residual stress prediction of production components such as the Ares I-X. The code is an analytical solution based on the Rosenthal solution of a point heat source moving in an infinite domain at a constant direction and speed. Without additional treatment, the Rosenthal solution cannot be used to calculate the temperature profiles for industrial applications. Modifications to the Rosenthal solution [11] were first made by Rybicki and Stonesifer to predict weld pass temperature histories for the finite element residual stress analysis of girth welded pipes as described in References [12] and [13]. Good agreement between temperature data and predicted temperatures were found by Rybicki and Stonesifer. In addition, the resulting computed residual stresses were in good agreement with residual stress data. Based on this work, the modified moving heat source method was used and expanded for use in VFT. To simulate the surface of a component, CTSP uses the imaginary heat sources reflected on the surface of the component to achieve the equivalent heat conduction. Meanwhile, CTSP uses the "negative" heat sources starting at the time of welding end to simulate the stop of the welding and transients [8-13].

Using these techniques, CTSP is able to simulate typical weld joint types such as groove joints, lap joints, T-fillet joints, traverse complex welds, and multiple weld paths. Figure 4 shows the validation of CTSP against the experimental measurement. This example is for a tee-fillet weld similar to the Ares weld models to be discussed later. During the development of the VFT code, numerous validation examples were used to drive the code development (many can be found in References 1-13 and the many references sited therein). These validations were made with both thermocouple measurements of test components and full numerical thermal solutions using DFLUX user routines in conjunction with the commercial finite element analysis code ABAQUS®. The details on CTSP have been well documented and reported in the literature. Only its advantage and essential features are highlighted as follows.

- The computation time for CTSP is much faster than that of the numerical solution. Depending on the complexity of the structure, a thermal calculation using CTSP can be 100~1000 times faster than a finite element analysis. One reason for this significant speedup is that CTSP avoids the calculation of the whole structure and only focuses on the local region around the heat-affected zone.

- CTSP solutions for coarse meshes are very accurate for predicting the temperatures at the coarse node points. These temperatures provide accurate through thickness temperatures, which are critical as input for providing accurate distortion and residual stress predictions.

- The input and analysis procedure is much simpler than those using numerical method. This is especially true for large structures with multi-pass welds.

Perhaps the only area where a numerical solution has an advantage compared with CTSP is cases where the material micro-structure needs to be predicted as modified by welding.

Structural Solution and Weld Constitutive Model

The structural model (UMAT) was developed based on ABAQUS commercial finite element codes by implementing a special materials module, which includes a constitutive law that permits stress relief due to weld melting/re-melting effects, strain hardening effects, large deformation mechanisms, rapid weld metal deposition features, phase transformation plasticity (based on the Leblond model [2]), etc. Experience clearly suggests that uncoupled thermal/structural solutions for weld problems are accurate in all weld models. Moreover, visco-plastic (or creep) effects are not important since the time spent in the creep regime during welding is negligible. However, creep effects are permitted and are often used to model heat treatments of steels and stress relief due to heat treatment. The constitutive model library within the UMAT permits isotropic, kinematic, and mixed hardening (Lemaitre-Chaboche). Here isotropic hardening is used, which tends to produce upper bound stress results. Many more details of the VFT code, with many example solutions, can be found in References [1-10] and in the many references therein.

Weld Model Validation

There was no direct validation of the computational weld modeling procedure and results used to produce the results in this report for the Ares I-X flange to shell welds. However, the Virtual Fabrication Technology (VFT^{TM}) procedures and weld modeling code used here to model the Ares tuna can welds has been validated on many different welded structures. The library of validation cases is more than fifty total. One example of the thermal model validation was presented above and here we briefly discuss validation of the distortion and residual stress prediction capability of the weld model. Direct validation on the Ares tuna can welds has not been performed since distortions and residual stresses were not measured for the final weld procedures. Here we present a validation case for distortions and residual stresses separately.

Distortion Validation Case

One issue not explicitly considered here, but which can be important, is the distortions of the Ares I-X welds. Often control of distortions by using designed weld processes that control distortions can save a large amount of money. The welding process induces weld residual stresses which in turn cause distortions. As the weld pass is deposited, it heats up the adjacent base material, which attempts to expand. This expansion is prevented by the bulk structural material and hence it undergoes some degree of compressive plasticity during this expansion. As cooling of the pass occurs, the weld metal and the adjacent heated base metal attempts to shrink during cooling. This process leads to tensile stresses *in the weld in the direction of torch movement*. The stresses in the other two directions are more complicated and can depend on weld joint constraint, geometry, weld and base

material, piece thickness, etc. Often the residual stresses and corresponding distortion predictions can be counter intuitive, especially in large complicated geometries and weld joints. It is important to have confidence in the model predictions. During the development of the VFT weld code, validation was made on numerous welded components. VFT is now used with confidence by a number of organizations including throughout the Caterpillar's worldwide business units.

Figure 5 shows a multi-pass welding mock up sample of the lifting component for a mining machine. This represents one of the early application examples performed by Caterpillar during the weld model development phase so that measurements were made. Thermocouples and laser displacement sensors were used to monitor the transient responses of the component during the welding (temperature validation of the CTSP code for this component is not presented here). This example was also presented in the VFT validation manual and in Reference [4]. The spikes in the temperature profiles and distortions represent roughly the responses of the structure to multiple passes of the welding. The simulation faced significant challenges in 1998 when computer resources were not as advanced as today as follows.

- The size of the sample is about 500mm by 1000mm in size. The total length of the weld is more than 20 meters. Including the inter-pass cooling time, the total welding time is more than 5 hours. As seen in the left in Figure 5, two different weld joints were used. The center circular weld was a 7 pass butt weld and the side welds were three and five pass short tee-fillet welds.

- Material melting at the elevated temperature had been one of the major challenges in welding simulation at this time. Modeling melting and solidification, which causes the relaxation and recovery of elastic and plastic strains, is very complicated and not fully understood. Moreover, multi-pass welding imposes the challenge of tracking material behavior during the re-melting.

- Hexagonal or brick element is the preferred element type for solid meshing. Brick elements would reduce the number of degrees of freedom and can avoid over stiffness (locking) of tetrahedral elements. However, building a brick element model for this mock up sample is not an easy task, although its geometry is considered fairly simple compared to other real components.

Today, ten years after this early validation case was performed, solution times are much more rapid, but the predicted results are the same. As seen in Figure 5 the distortion predictions are within 10 % of the laser sensor measured distortions. It is emphasized that there are numerous other validation examples presented in the literature for illustrating the ability of VFT to predict distortions (see [1 – 10]] for instance). The distortions are entirely due to the weld induced residual stresses caused by welding. This is very good considering the well known weld variability known to exist in the field. Welding simulation for industrial applications including the Ares vehicle also needs to deal with the inevitable process variability in a shop environment. Different from a controlled lab experiment, welding in shop floor could vary from time to time and from

welder to welder. Usually welding procedure specification represents the normal welding parameters while the true parameters in the shop could vary significantly, including heat input, welding speed, weld size, welding sequence, inter-pass cooling and even part fit-up, enough to cause the grief in a simulation. Finally, a recent example of using the VFT computational weld modeling tool (with validation) of a large stiffened ship panel which had 194 welds to be managed can be found in [14].

Residual Stress Measurements

The validation of computational weld models using distortion predictions is not controversial since weld induced distortions can be easily measured. However, measurement of *weld residual stresses* is rather controversial and is the topic of much interest at present. Before presenting validation examples for the weld residual stress predictions, it is worthwhile to discuss some of these measurement issues first. Suffice it to say that measured residual stresses are a source of significant error and this must be kept in mind when validating weld models.

There are a number of methods that have been developed and are used for measuring residual stresses in welded components. These methods can be non-destructive (for instance x-ray diffraction) or destructive (for instance hole drilling). All methods of measuring weld residual stresses attempt to measure the elastic strain and then calculate the residual stress using elastic constants. For the destructive methods this can induce error since it must be assumed that elastic unloading occurs while the weld piece is destroyed (e.g., hole drilling, saw cut, etc.). Because of this there is always a question regarding the accuracy of weld residual stress measurements – perhaps just as much as with the predictions. Before showing some residual stress validation cases it is useful to discuss some of the measurement methods and their limitations first.

Some of the more popular measurement methods are discussed in the following. These include deep hole drilling, neutron diffraction, contour method, and surface methods such as x-ray diffraction.

- Deep Hole Method (DH). This variant of the old ASTM hole drilling method which is considered more accurate. This method involves drilling a 3 mm pilot hole in the specimen at the area where the measurements are to be made. The hole diameter through the thickness is measured (at .2 mm increments) using an air probe measurement device. An annular ring is then cut around this hole (about 10 mm in size), thus releasing the residual stresses in the radial direction (direction perpendicular to the drilled hole). The original pilot hole is then re-measured; strains are calculated from the change in displacements. *It is important to note that distortions are measured and these are converted to strains, hence stresses, using various assumptions.* The key assumption here is that the cuts only result in elastic unloading, and therefore, the stresses calculated from the inferred strains result in a unique stress solution. Coupling between stress components is not possible (i.e., the stresses in a direction parallel to the drilling direction cannot be considered). Because of the size of the hole drilled, these measurements represent averages over the region of the hole and steep strain

gradients cannot be accurately measured. The DH is the only practical method for through-wall stresses in wall sections greater than about 40mm and it is not recommended for sections less than about 20mm thick. All strain relief methods (such as DH) begin to break down when the stress levels exceed about 2/3 yield. Note stresses in weld metal usually exceed this threshold. The DH is also in trouble under conditions of high tri-axiality such as occur in the Ares I-X weld.

- The Contour Method (CM). This is a promising method but it is relatively new. Developed recently by Los Alamos National Laboratory, CM consists of making a saw cut through the specimen at the location where the through thickness residual stresses are needed. The displacement at the cut location is carefully measured, usually using a coordinate measurement device. The finite element method is then used to apply the measured displacements at the cut location and the stresses are then easily calculated. As with the deep hole drilling method, *it is important to note that distortions are measured and these are converted to stresses.* This is a simple destructive method to obtain weld residual stresses, but requires very accurate distortion measurements – something often difficult to achieve. It will give erroneous results when there is plasticity during cutting and it cannot deal with complex structures such as the Ares I-X weld.

- Neutron Diffraction (ND). The Neutron Diffraction (ND) method relies on elastic deformations within a polycrystalline material that cause changes in the spacing of the lattice planes from their stress-free value. This method requires the use of a nuclear reactor to dispel neutrons and can be quite expensive. Measurements by ND are carried out in much the same way as with XRD (see below), with a detector moving around the sample, locating the positions of high intensity diffracted beams. A collimated neutron beam of wavelength γ is diffracted at an angle of 2θ by the polycrystalline sample, collected, and lattice differences measured. The inter-planar distance can be evaluated using Bragg's law, and the corresponding lattice strain can be evaluated. The stress values can, therefore, be determined from these strain readings using appropriate mathematical formulae. ND can only give reliable through-wall stress measurements in sections less than about 40mm thick (depends on neutron source and your patience and budget). ND measurements from a pulsed source are most reliable. Experienced practitioners must do the measurements. Careful measurement of the stress-free lattice parameters are used as a reference condition once strain measurements are being made. Residual stress measurements in weld metal are very difficult because of high texture, multiple phases and chemistry variations. ND measurements can be very expensive if you have to pay full commercial rates for neutron beam time and the specimens have to be small enough..

- X-ray Diffraction Surface Method (XRD). This method is well established and is similar to ND methods except x-rays are used. For this reason, XRD is portable and relatively cheap. However, surface measurements (such as XRD) reveal little about what is going on inside the structure where steep near-surface stress gradients exist , either owing to machining, or heat treatment or from the welding.

Thus surface measurements can only augment other measurement methods and must be done with extreme care and understanding. However, XRD measurements are well established and commercial organizations perform these measurements routinely.

There are other methods such as synchrotron diffraction (which is relatively new), trepanning, ring core, optical microscopy, among others. All of these methods can be useful, but require experienced people to perform the measurements. References [15, 16] discuss the strengths and weaknesses of measurement methods in more detail. Even with experienced specialists making the measurements, there is significant scatter that can result in such measurements. Take for instance the example from Turski, Bouchard, et al [16]. A simple, single pass, bead on plate weld is made as seen in the upper right inset in Figure 6 with dimensions shown. The material was a well characterized Type 316L stainless steel. The plot to the left in Figure 6 shows measurement of transverse (perpendicular to weld direction) residual stress made by five different organizations using three different methods (3 used neutron diffraction, 1 used the contour method, and 1 used deep hole drilling). The difference in the magnitude of the residual stress is marked although the general trend is similar between the measurements. This illustrates that the magnitude of residual stress measurements is subject to wide variations even for such a simple single pass specimen.

Residual Stress Validation

Despite the apparent variability in residual stress measurements, which illustrates the need to augment weld model validation with distortion measurements, there has been extensive validation of the VFT weld modelling code (see References [1-10] and those sited therein). Figure 7 illustrates the comparison of predicted residual stresses for a 'bead on plate' example which is similar to that made by Turski et al [16] and discussed in relation to Figure 6. The dimensions are shown in the top illustration and the material is a mild steel similar to the AISC A36 designation. Here the residual stresses were measured using the surface measurement technique, x-ray diffraction, and it is seen that the comparison is rather good considering the discussion regarding variability in measurements in the previous section. In Figure 7 the '0' and '90' designations represent parallel to the weld direction and perpendicular to the weld direction, respectively.

Bimetal Weld Validation. This weld model validation section is completed by showing the validation of the weld model with a rather complicated bimetal pipe weld where residual stress measurements were made using neutron diffraction. This is a very complicated weld fabrication which is detailed in Figures 8 and 9. The pipe was fabricated and the residual stress measurements were made as part of the European Union Network for Evaluating Steel Components (EU-NESC) program [17]. This work represents a 'computational round robin' problem for evaluation of various computational weld models and their accuracy.

The component illustrated in Figures 8 and 9 represents a bimetal weld used in nuclear piping. This type of welded pipe typically is made from the reactor pressure vessel to pipe running to the steam generator (a 'hot leg' pipe). As seen in Figure 9 at the top,

A508 vessel steel is welded to a 316 stainless steel pipe using stainless steel electrodes. A508 steel is quite similar to A516-70 steel used for Ares I-X (similar material properties and metallurgy) used in the Ares I-X vessel and both steels are frequently used in nuclear pressure vessels. This and similar bimetal welds in pressurized water reactors (PWR) has caused concern in recent years due to weld residual stress induced stress corrosion cracking that has occurred in a number of plants worldwide. As such, it has been the subject of intense research in recent years (see for instance References [18-19]). This research work has led to an improvement in weld model codes including the VFT code used here.

Referring to Figure 8 and step 1, the A508 steel is first 'buttered' with the stainless steel electrode material. This pipe is rather large diameter with a thickness of 69 mm (nearly 3"). The buttering was applied in 68 passes and the model was axis-symmetric in this case. It has been shown that axis-symmetric solutions produce upper bound weld residual stresses in pipe [18, 19]. Note that the Ares I-X vessel is of much larger diameter has a gusset stiffener, and a stiff ring being welded to the shell, making the use of an axis-symmetric model not of much value here. After the buttering, material is machined from the pipes as illustrated in steps 2 and 3 in Figure 8 with the dimensions after this step shown in step 3. This was modelled using the material removal option within ABAQUS. In step 4 (Figure 9) the stainless steel pipe pieces were added and 87 weld passes were deposited. All 87 passes were modelled. Note also in step 4 that the pipe was put through a post weld heat treatment at a maximum temperature of 598 C. The heat treat consisted of slow heating for 8.5 hours, holding at temperature for 6 hours at 598 C, and then slow cooling for 9 hours. All steps were modeled assuming that partial stress relaxation occurred due to creep at these temperatures. It is emphasized that this final step is not performed in most US built PWR's. The amount of stress relaxation that occurs during this heat treat depends strongly on the creep properties used during the modeling of the PWHT process. Finally, steps 5 and 6 illustrate the final machining process which was also modeled. The final pipe dimensions are shown in step 6. It was this section of pipe which had the residual stresses measured using neutron diffraction.

Figure 10 compares predictions of both axial and hoop direction (hoop is in the direction of welding) weld residual stresses in the center of the butter region from the final pipe OD (which is at 226.5 mm) through the thickness. It is seen that the comparison is quite reasonable. The plots on the right show the predicted and measured residual stresses through the weld centerline. This was more complicated than a typical weld since there were two machining processes which had to be modeled and also the final post weld heat treatment. The post weld heat treatment was modeled using creep properties found in the literature and the accuracy of these properties in not known. The EU-NESC report [17] states the following: "In characterizing the measured residual stresses present in the EU-NESC bimetal weld, the different measurement techniques proved complementary. The neutron diffraction data provided a 3-D mapping of the strains and stresses, *although the thickness of the weld and its crystallographic texture meant that only the hoop direction data is fully reliable. Moreover … the reliability of the neutron diffraction measurements for depths greater than about 35 to 40 mm is unreliable as well."* These measured points are circled with a red ellipse in Figure 10.

Figure 11 shows comparisons of predictions to neutron diffraction measurements at several locations. The left side plots show axial and hoop residual stress measured 4.25 mm below the pipe OD surface. The zero location in these plots represents the weld centerline. The right side plots likewise show hoop residual stress comparisons at 21 and 29.75 mm below the OD surface. Although the magnitudes do not always compare exactly, the plot trends compare very well.

There are a number of additional validation cases which illustrate the accuracy of predictions using the VFT weld model in the sited references in addition to the examples shown here. Hence, despite the fact that no measurements were made on the Ares I-X tuna can weld component, this provides us with confidence that the predicted weld residual stresses shown in the following sections can be used with confidence.

Ares I-X Weld Model

The key Ares I-X welds and corresponding results are presented in this section. During this work there were a number of different weld concepts, procedures, and joint types considered. For completeness the results of many of these analyses are presented even though some of the concepts were rejected because the residual stress field produced was not advantageous. In general, it was found that minimizing the weld residual stresses near the inner diameter of the shell to flange weld resulted in the largest critical initial flaw size (CIFS), i.e., axial tensile residual stresses at the shell ID near the fillet weld are not desirable and should be avoided. This is because the critical service loads lead to a worse case crack growth scenario for ID cracks. Details of the contributing stress analysis [20] and actual CIFS assessment details [21], as well as the overall report may be found in [22].

The heat and corresponding weld shrinkage caused by welding lead to residual stresses. These residual stresses are localized to the region of the weld. The residual stresses also cause distortions which can affect fit up and tolerance requirements throughout the component structure. The residual stresses in the shell and flange prior to welding were not considered in this analysis. It is known that the shell and flange forming processes do induce a residual stress field in the parts prior to fit-up and welding. There is evidence that longitudinal seam welds used to close submarine size cylinders require forming residual stresses to be included as initial conditions for increased accuracy. This was recently observed in some submarine fabrication weld analyses and corresponding welded component observations [23]. However, the circumferential welds modeled here are not expected to require the initial forming stresses in order for accurate weld stress predictions because the key weld is circumferential.

Weld Geometry

A ten-degree segment of the tuna can shell and flange was modeled as shown in Figure 12. To reduce the solution degrees-of-freedom, a 96 cm length of the can was chosen for analysis, and the remainder of the acreage of the can was omitted. The can was modeled with ABAQUS C3D8R solid elements. A gusset with a ‘mouse hole’ was included to capture the correct stiffness. In the model, the gusset weld itself was not explicitly

modeled. Because of the presence of the gusset, the problem is not axis-symmetric. However, some axis-symmetric analyses were performed during sensitivity studies. The boundary conditions shown in the left hand side of Figure 12 were chosen to prohibit rigid body motion of the flange ring segment during the weld process. At both ends of the model (0- and 10-degree locations), free boundary conditions were imposed. Two sets of analyses were performed to verify the local nature of the weld residual stresses. One analysis was performed where cyclic symmetry boundary conditions were imposed at the 0- and 10-degree locations. Another analysis was performed where the omitted acreage of the can was included and modeled with shell elements tied to the solid elements at the interface. As expected, the weld residual stress influence was local to the weld joint and hence neither the cyclic boundary conditions nor inclusion of the acreage of the can had an important effect on weld residual stress. Finally, as seen in the right of Figure 12, four meshes of increasing refinement was used to verify that the solution converged (the course, fine, and the two finest models, respectively). The model labeled 'finest model 2' was used for the analyses that were used for the final CIFS solutions.

The inset to the lower right of Figure 12 shows the details of the weld joint. The joint was either a single-vee or a 'double-vee' with a fillet weld deposited along the inner diameter of the shell- surface interface. The thick flange ring stiffness and the gusset had a profound influence on the weld residual stresses compared to a simple shell groove weld (as in a large diameter pipe). The welds were made using 5 to 7 weld passes depending on the sequence. The range of weld parameters were: Amps = 200– 215, Volts = 25–26, and weld speed = 4–5 mm/sec. The thermo-physical properties used for the thermal analysis and the temperature dependent stress strain curves used for A516-70 steel are presented in References [18] and [24] and Figure 14. Full moving arc analyses were performed since 'lump pass' assumptions, where the passes are deposited at once, were found to produce less accurate results.

Figure 13 illustrates the locations where the weld residual stresses were compiled and used in the critical initial flaw size (CIFS) evaluations. As seen in the lower left insert, the stresses were evaluated in the shell at the toe of the fillet weld from the ID to OD of the shell. Axial (perpendicular to the weld direction) and hoop (the weld travel direction) residual stresses were compiled at locations illustrated in Figure 13. Cut plane 0 runs through the first full hole, cut plane 1 is through the second hole, cut plane 2 is at the gusset 'mouse hole' location, and cut plane 3 is on the other side of the gusset near the weld stop location as illustrated in Figure 13. The stresses at other locations (including the possibility of cracks in the ring) were also considered for the CIFS analysis, but it was determined that circumferential crack growth (caused by axial shell stresses at the toe of the weld) were most critical. Many of the residual stresses shown in the following are at Cut -2 of Figure 13.

Material Properties

Figure 14 shows the weld parameters, thermal properties, and weld material properties used for the analysis. The tables shown in Figure 14 present the weld parameters used for the welds, the thermal physical properties used for the thermal weld analysis, and the temperature dependent material properties curves used for the structural portion of the

analysis. Thermal physical properties do vary slightly with temperature. However, within the framework of the CTSP thermal solution procedure, which is closed form, these properties must be independent of temperature. Comparisons of CTSP solutions with numerical (which used temperature dependent properties) thermal solutions shows this assumption to be very good. The temperature dependent stress-plastic strain properties of A516-70 steel were obtained from Reference [23, 24]. Note that properties are needed to near melting for proper weld analysis since melted material is considered by using a very low stiffness (see [1-10]).

Weld Sequences

There are a number of factors that determine the final weld residual stress and distortion state. Weld modeling is often used to design weld methods to either minimize or control residual stresses and/or distortions. Some of the many techniques that have been developed are discussed in detail in Reference [5]. Some of these factors include weld sequence, weld groove geometry, weld parameters, weld piece constraint, tacking methods, use of heat sinks, thermal tensioning, weld electrode used, and special methods such as pre-cambering, pre-bend, post weld heat treat, among many others. For the Ares I-X work considered here, the weld groove geometry and weld sequence were key contributing factors in developing a favorable or unfavorable weld residual stress state. The weld definitions and weld sequences presented here were mainly driven by the NASA program team. A key conclusion from this weld modeling work, which is discussed in detail later, is that the final pass should be deposited at the outer diameter (OD) of the shell to flange weld. For both joint geometries (single and double-vee) shown in Figure 15, the weld sequences in Figure 15 a, b, and d should be used and the Figure 15c sequence should be avoided. Note that the weld passes here are idealized with square elements. This has a second order effect on the final residual stress pattern. The Figure 15c sequence results in a high tensile weld residual state at the ID of the shell. This results in reduced fatigue life and a smaller CIFS.

The original weld sequence shown in Figure 15a was single-vee weld geometry. The fillet weld is deposited first and then the weld joint is sequentially filled from the ID to the OD. This type of weld joint will typically result in larger out of plane weld distortions of both shell and ring since the weld shrinkage progresses from the ID to OD as each pass is deposited. Figure 15 (b-d) shows the weld sequence for a balanced double-vee weld. It is seen that the weld is balanced about the mid thickness of the shell, which tends to minimize distortions in such welds. This is further discussed later.

Weld Residual Stress Predictions for 6-pass Case

The CIFS assessment of the Ares I-X simulator evolved over the time of the assessment as the design team made changes to many structural features including joint geometry, weld joint type, weld sequence, etc. This led to many different weld analyses *during* the course of the program. Early in the program the weld joint was a single-vee as illustrated in Figure 15a. For this case, the fillet weld was made on the ID first, followed by filling through the shell thickness with the final pass on the outer diameter (OD). This type of weld can lead to distortion problems since more weld metal is deposited at the shell OD. A ‘balanced’ sequence with six passes was then considered as in Figure 15b. This type

of sequence reduces the magnitude of weld induced distortions because the final pass is deposited at the OD. As will be discussed subsequently, the final weld pass location determines the peak tensile axial weld residual stress location for this geometry. It turns out [21, 22] that circumferential cracks in the shell which are driven by axial stresses near the toe of the fillet weld (Figure 15) are the critical crack type for the Ares I-X. Moreover, a circumferential crack starting on the ID of the shell and growing to the OD is also worst case scenario [21, 22]. This type of crack is driven by service loads along with weld residual stresses. Hoop stresses are 'in the direction of the weld arc movement' (Z-direction in Figure 12) and axial stresses are perpendicular to this (Y-direction in Figure 12). Hence, here we mainly focus on axial stresses although other components of stress are sometimes reported. This study determined that the final pass, which should be located on the OD of the shell as in Figure 15d is desirable in order to increase the size of the CIFS. The final pass location is more important than whether 6 (Figure 15b) or 7 passes (Figure 15d) are deposited. Therefore, results for both the 6 and 7 pass cases are presented.

Weld Residual Stresses for Final Pass on Shell OD

Figure 16 illustrates the Von Mises and axial weld residual stress profiles for the balanced double-vee weld sequence of Figure 15b. The stresses vary with position because of the moving weld arc, the stiffness supplied by the gusset, the in-plane stiffness of the ring, and to some extent, the holes in the flange. The effect of the ring stiffener in preventing full radial shrinkage and the gusset stiffener stresses clearly illustrate this. Figure 17 shows the axial weld residual stresses at each of the four cut locations shown in Figure 13. The axial stresses at cut locations 1 and 2 are largest in magnitude. Interestingly the stresses are compressive at the shell ID, and go to tension near the middle, and then go to near zero (Figure 18 also) near the outside of the shell. From the plots in Figure 17 and the upper left contour plot in Figure 18, one can clearly see that the axial stresses are tensile on the OD above and below this location. This 'tensile stress band' is illustrated in the upper left plot in Figure 18. In effect, the tensile band goes around the point along the 'black line bands' in the upper left inset in Figure 18. This is due to the unique constraint in the Ares I-X weld and the competition between axial and radial shrinkage and the stiffener constraint (discussed later). In addition, Figure 18 is a line plot of the weld residual stresses at the four cut locations in the finest model. These are axial stresses plotted from the shell inner diameter through the wall thickness (12.7 mm or 0.5-inch) at the fillet weld toe as illustrated in the inset of Figure 18 along the white arrow. These are the stresses that are used for the CIFS analyses. Axial stresses can contribute to circumferential cracks in the shell at the toe of the fillet, which is the key concern for the tuna can shell welds.

As a simple rule of thumb regarding weld analyses for cases where there are not many weld passes (here only 6 total passes) and a stiff local structure (such as the Ares I-X), the final weld beads tend to control the location of axial tensile weld residual stresses. (The 'hoop' weld residual stresses in the direction of welding are usually fully tensile for shells of this thickness). The weld bead deposition effect is illustrated Figure 19, where the axial weld residual stresses for passes 3 to 6 are shown at the Cut-2 location using the finest finite element model. The weld sequence is illustrated in the left inset of Figure 19.

One can see that after passes 3 and 5 are complete, the tensile axial stresses are on the inside diameter of the shell. After passes 4 and 6, the tensile stresses move to the outer diameter of the shell. Each successive pass increases the weld residual stress magnitude as well.

The tuna can weld analysis of the double-vee geometry was performed using more than four different mesh refinements (some of which are illustrated in Figure 15). This was done for two reasons: (i) to ensure the solution converged and (ii) to ensure there were no solution errors since the analyses were performed separately and independently. There were some differences in the weld residual stress magnitudes using the different mesh refinements, but the stress patterns were very similar. Figure 20 illustrates this for the cases of 8 elements and 12 elements through the shell. While the magnitudes do vary slightly, the effect is small and verifies that the solution has converged. Similar results were obtained with two other meshes of different refinement also including more refinement in the ring. The results from the 'finest mesh 2' solution of Figure 12 were used for the CIFS analysis.

Pipe Weld versus Ares I-X Weld

The results shown here are now compared to what would be expected in a shell weld without the ring flange stiffener. Many studies of residual stresses in pipe welds have been made over the years in the power generation and transmission pipeline industries. For example, tensile weld residual stresses in pipe along the inner surface can lead to serious stress corrosion cracking (SCC) problems. This was prevalent in boiling water nuclear reactors in the late 1970's where heat affected zone SCC led to the development of weld procedures to induce compressive weld residual stresses along the inner surface of these pipe. Early versions of computational weld models led by Rybicki et al [13, 25-26] were used for this development. In fact, the VFT code has its roots in these early weld modeling codes. In the absence of the ring flange and the gusset, the configuration would be analogous to a large diameter girth welded vessel. For a shell of this thickness (12.7 mm), the welding of a pipe would produce tensile weld residual stresses on the shell inner surface (see Brust and Dong, Reference [27] for a general summary of weld induced residual stresses expected in regular geometries such as pipe).

Consider a summary of weld residual stresses which develop in pipe of different thickness (this is a summary of some results presented by Fredette and Brust [29]). Figure 21 shows the axial weld residual stresses which develop in pipe of different thickness (the mean radius to pipe thickness ratio for all pipes here is R/t =10). It is seen that for the thin pipe (t = 7.5 mm) the axial weld residual stress distribution is a 'bending type' with tension on the pipe ID and compression on the OD. The middle thickness pipe (t = 15 mm) produces compression on the OD, with tension (or near zero axial stresses) of a lower level on the ID. The thick pipe (t = 22.5 mm) the residual stress is tension on the OD, compression at mid thickness, and tension again on the ID. The middle thickness pipe with a thickness about 15 mm appears to be near the transition between a 'bending type' and a more complicated 'stress reversal' type of residual stress distribution.

The axial weld residual stresses in girth welded pipe is caused by two competing mechanisms. Referring to Figure 22, the radial shrinkage of the weld bead is analogous to applying a 'ring load' to the pipe, which produces bending stresses through the shell wall – tension at the ID and compression at the OD (for relatively thin pipe). On the other hand, the axial shrinkage of the weld bead tends to produce axial tension at the location of the final weld passes which are deposited on the pipe OD. Referring to Figure 22, it is clear that, for thin wall pipe, the radial shrinkage produces a type of 'global bending' which dominates, leading to tension on the ID and compression on the OD. As the pipe wall becomes thicker, the radial shrinkage effect weakens and a combination of radial shrinkage and axial weld shrinkage leads to a more complicated weld residual stress distribution. The transition from a thin to thick pipe weld residual stress distribution appears to be around 14 to 18 mm (depending on R/t ratio) [13, 27]. Similar results, with experimental residual stress data, are reported for girth welded pipes in the paper by Rybicki, McGuire, Merrick, and Wert.[28] Residual stress data and the finite element analyses of Reference [29] show that as the pipe wall thickness increases, the weld residual stresses on the pipe ID become more compressive because of the increased bending stiffness.

For a weld sequence as in Figure 15b or 15d, where the last pass is deposited at the OD, this radial shrinkage would result in tension on the ID and compression on the OD for this thickness shell (12.5 mm). However, free radial shrinkage of the shell is prevented by the stiff ring and the gusset in the Ares I-X weld. In fact, some twisting of the ring stiffener is expected during deposition of the final passes near the OD due to the off-center (compared to the ring centerline) shrinkage of the weld. Hence in the Ares I-X shell, there is a competition between radial and axial shrinkage, with axial shrinkage winning the battle for the most part. For the Ares I-X vehicle with the final pass deposited on the OD, there is compression at the ID, tension in the middle, and a small amount of tension at the OD, as shown in Figure 17. The tension on the OD for this case is more complicated and stretches in a 'band' as seen in Figure 18 inset. This is the result of the additional competition of the stiff flange ring and the gusset. As such, the weld residual stress distribution in the Ares I-X is not intuitive. A number of other studies, including some axis-symmetric analyses, were performed to examine and prove this effect in detail.

Weld Constraint and Fracture

The weld process can produce a residual stress state in the weld joint that increases the constraint thereby reducing fracture toughness. It is well known that plane strain fracture toughness is lower than plane stress because the amount of plasticity that can develop under plane strain conditions is reduced. The development of direct relationships between constraint and fracture toughness is a topic of fruitful research at present in the fracture community. However, it is known that for a given material the higher the tensile constraint in the joint the lower the toughness. Figure 23 shows the constraint (hydrostatic stress measured as $\sigma_{kk}/3$, where σ_{ij} represents the stress tensor) and the Von Mises stress through the shell at the Cut-2 location. It is clear that there is significant tensile constraint near the mid thickness of the shell. Because yielding in metals is independent of hydrostatic stress it is possible for the component stresses to be higher

than yield (sometimes significantly). The hoop stresses are higher than the room temperature yield stress of 345 MPa (50 ksi). The maximum von Mises stress at this location is 483 MPa, the hydrostatic stress is 323 MPa, and the hoop stress is 600 MPa at x/t = 0.5.

Weld Sequence Effect

Figure 24 illustrates the importance of weld sequence in determining the final weld residual stress pattern for the tuna can shell-to-flange weld. The balanced sequence for the double-vee weld case is shown in the upper right insert. This balanced type of weld sequence will tend to minimize weld distortions. A weld sequence is shown in the lower right where the outside diameter welds are performed first followed by the inside welds. From Figure 24 it is seen that the axial weld residual stresses change from compression on the inner diameter (ID) for the balanced sequence to tension on the ID for sequence 2. The hoop stresses are also affected. The crack growth is expected to be different for these two markedly different weld residual stress patterns. It turns out that the residual stress pattern for the balanced sequence with the final pass on the OD is most advantageous for the Ares I-X shell to flange ring weld [21, 22]

Edge Effects and Boundary Conditions

There was concern that the free boundary conditions at the 0-degree and 10-degree locations (see Figure 25) might affect the predicted weld residual stresses. The lower left insert in Figure 25 illustrates the boundary conditions used for this case. The axial stresses are plotted in Figure 25 at the Cut-0 and Cut-1 (Figure 13) locations and illustrate that the edge boundary conditions are not important here because welding is a local effect. The stresses very close to these fixed locations do differ significantly from the free case but away from the edges the effect is of second order. For the critical weld residual stresses under the 'mouse hole' below the gusset, where the CIFS assessment was made, the edge effect is negligible.

Weld Groove Geometry Effects

Analyses were also performed for the single-vee weld sequence shown in Figure 15, upper left inset. This shows a single-vee weld groove where the ID fillet weld is deposited first, followed by sequentially completing the weld from the inside to outside with the final pass being pass 7 deposited on the shell OD. Figure 26 shows the through thickness axial weld residual stresses at all four cut locations. Comparing this with Figure 18 reveals that the residual stresses for the single vee analysis do not vary as much with position as those for the double-vee case. Figure 27 shows a contour plot of the residual stress distribution at the Cut-2 location with the three different mesh refinements used. Figure 28 shows the line plot results using all three mesh refinements (Figure 12). It is seen that for the single vee analysis there is more dependence on mesh refinement compared with the double-vee, although the coarse mesh is rather crude. This may be in part due to the fact that it was more difficult to model the weld pattern definition for the single-vee in the coarser models. Moreover, more weld material is deposited with the single-vee case at the OD. Figure 29 compares the single-vee and double-vee residual stress distributions. From the standpoint of CIFS the double-vee geometry is preferred.

Effect of Load Shake Down

The decrease in fatigue life caused by weld residual stresses are mainly caused by the higher mean stress and constraint induced by the weld stresses. The fracture response will be lowered since the weld residual stresses also contribute to the stress intensity factor – especially in relatively brittle materials. The A516-70 steel used here is relatively ductile so that the weld residual stresses and strains are likely 'washed out' during an overload failure and will contribute less to reducing the fracture response. Weld residual stresses will play a major role in stress corrosion cracking. However, SCC is not a concern here.

The service loads that are applied after weld fabrication will often cause the weld residual stresses to 'shakedown' to lower values over time. This effect is examined here for the tuna can shell to flange weld. Figure 30 illustrates the loads and boundary conditions used for the shakedown analysis. The modeling process is described below.

- Perform the weld analysis. This was for the 6-pass double vee geometry with the balanced weld sequence and final pass on the OD.
- Add additional boundary conditions as seen in Figure 30. As illustrated by the 'blue triangles' which represent the constraint applied to the top of the bolt holes in the '2-direction' or pressure load direction. These displacements were applied in such a way that they were kept at the value of the displacement after welding was complete, i.e., there is no additional displacement permitted in the '2-direction' after application and removal of the load. (This is the *BOUNDARY, FIXED option of ABAQUS). This was done to simulate the bolt constraints. Note that the weld process induces distortions in the flange. For one analysis (not shown here) these distortions in the flange were eliminated (or made zero) prior to adding the pressure load. This simulates fit up constraints that may occur due to tightening the bolts prior to load application. This has a marked effect the final weld residual stress state and could be included in another analysis in the future. Results are not shown here because the present model is not considered accurate enough to account for these bolt loads at this point. The Ares I-X service loads [20], which produces local stresses at the fillet toe, combine with weld residual stresses and are used for the fatigue assessment in [21, 22]. Reference [20] shows that these bolt loads, when tightened so as to mate the two flange surfaces, do produce large stresses. This was independently verified here and illustrates that distortion control of the flange after welding can be an important weld control factor. Distortions are discussed later.
- Apply the pressure load and then release the load. Only one pressure cycle is applied here. A number of pressures were considered with two pressures (22 Mpa (3.2 ksi) and 86 Mpa (12.5 ksi) shown here) were applied and released. Since these were applied after the weld modeling is complete, the complete history of welding stresses and strains are properly included in this analysis. The 22 Mpa pressure represents an equivalent pressure determined as part of the CIFS analysis cases, and represents a typical service load while the 86 Mpa load is large and is considered to accelerate the effect of load shakedown.

Figure 31 shows a global view of the residual stress state (axial in the shell or in the '2-direction) after welding and after the application and release of 86 Mpa. It is seen that the residual stresses relax after the pressure unload. The 86 Mpa pressure loading is larger than the actual equivalent pressure load (22 Mpa), but the relaxation effect is clearly evident.

Figure 32 shows the axial residual stresses at the Cut-2 location for all three cases. It is evident that the application of the equivalent pressure of 22 Mpa does have the effect of reducing the final residual stress pattern slightly after removal. One could imagine that if many cycles were applied, and some plasticity occurs locally near the weld during each load cycle, the weld residual stresses would shake down further. The results after application and release of the 86 Mpa pressure load does reduce the weld residual stresses at this location significantly. This suggests that the application of a 'proof load' to reduce the weld residual stress state in the shell to flange weld might be worthy of consideration. Indeed, proof loads applied to nuclear piping systems perform the same function.

Final Weld Residual Stress Predictions for 7-pass Case

The Ares 1-X weld procedures evolved during the program. Early on the single-vee geometry was used with a semi-automatic weld procedure with a non-balanced sequence as in Figure 15a. As the design changed and a better appreciation of the weld process needed to meet the CIFS design goals, the 6-pass balanced double-vee geometry with manual welding emerged as seen in Figures 15b emerged at the leading candidate. Finally, the balanced 7-pass sequence as in Figure 15c and 15d emerged as the leading candidate welds sequence, again using manual arc welding. The purpose of this section is to discuss the final weld sequence results that were used for the final CIFS assessment. More details of the weld process development for the Ares 1-X are discussed in detail in [22].

CIFS Assessment – Final Weld Sequence

Figure 33a shows the original balanced weld sequence that was designed for the Ares I-X. It shows that the final pass is deposited on the fillet weld at the ID. It will be seen that the sequence shown in Figure 33b, with the final pass on the OD, produces the optimum weld residual stress distribution for maximizing the CIFS. Figure 34 shows line plots through the shell wall thickness at the toe of the fillet weld that is used for the CIFS assessment in Reference [21]. The axial stresses for the case of the final pass on the OD are shown in the upper left of Figure 34 while the upper right plot is for the final pass on the ID. These stresses are plotted at Cut-0, -1, and -2. It is clearly seen that the axial stress distribution for the pass on the ID is compressive at the critical Cut-2 location (under the gusset) while it is tensile for the final pass on the OD. When these weld residual stresses are used as part of the CIFS study in Reference [21], the final pass on the OD produces the highest CIFS. Hence, our recommendation for the Ares 1-X weld is to require the final pass to be deposited at the OD of the shell. The hoop stresses for both weld sequences are also shown in Figure 34.

Figure 35 shows contour plots of the 7-pass final sequence for the case of the final pass deposited on the OD (the desired case). The top plot shows the contour plots after deposition of the sixth pass (7^{th} pass is not yet deposited yet). The left side shows a back view of the shell and ring at the Cut-2 location. The black ellipse on the left side plots shows the region of interest for the stresses needed for the CIFS assessment. The right side plots show the detailed stresses at the shell cross section. The clear importance of final pass location is clearly seen here.

Distortions for Final Weld Sequence Case

The main purpose of this weld modeling assessment of the Ares I-X was to obtain weld residual stresses to include in the CIFS assessment. This final section discusses the distortions that develop in the welded tuna can assembly. Figure 1 illustrates the 7 'tuna can' segments that must be bolted together (US-1 to US-7) to make the upper stage assembly. Figures 12, 13, and 30 further illustrate the regions of the required bolted connections. The welding process induces distortions in the ring and shell along with weld residual stresses.

Knight, Philips, and Raju [20] looked at the effect of distortions patterns on the stresses caused by bolting. When the ring is distorted, bolting the rings induces an additional source of weld residual stresses caused when the adjacent rings deform to properly seat as the bolts are tightened. Reference [20] looked at a number of different distortion patterns that have been observed in welded tuna can assemblies and determined that the corresponding bolt induced residual stresses can be significant. Here we take a brief look at this effect.

Figure 36 illustrates the predicted vertical displacements for the 7-pass final weld configuration. It is seen that vertical displacements are positive near the region of the Cut-0 and Cut-1 locations. When the bolts connect the upper and lower ring segments, these displacements will reduce until the upper and lower bolted rings come into contact. This induces significant weld residual stresses in the shell at the top of the fillet weld, as also shown in [20]. It was shown that the effect of only modeling a 10-degree segment, along with only a portion of the shell has little effect on the weld residual stresses. However, the distortions may be affected by neglecting the rest of the segment. This would have to be verified by modeling a larger segment (perhaps 360-degrees) with a coarse model. However, it should be clear that computational weld modeling can be used to develop weld sequences, constraints, and other residual stress and distortion control techniques to also minimize this effect. This would potentially reduce the fit up stresses and increase the CIFS.

Concluding Remarks

This report describes the weld residual stress analyses performed supporting the NESC Critical Initial Flaw Size (CIFS) assessment of the Ares I-X USS common tuna-can segments. Here, a series of weld analyses are performed to determine the residual stresses in a critical region of the USS. Weld residual stresses both increase constraint and mean stress thereby having an important effect on fatigue and fracture life. The results of this effort served as one of the critical load inputs required to perform a critical

initial flaw size (CIFS) assessment of the same segment. It is clear that careful design of weld fabrication procedures, including joint type, weld parameters, weld sequence, fabrication constraints, and distortions are very important to improve the life of welded fabrications.

Computational weld modeling is challenging because many of the processes of welding are highly nonlinear. Material melts and re-solidifies, very high transient thermal gradients are experienced, non-linear temperature dependent plastic straining and phase transformations can occur, among other sources of nonlinearity. A well validated computational weld modeling code, Virtual Fabrication Technology (VFT^{TM}), was used here to predict the flange to shell weld residual stresses. There was not direct validation of the model predictions for the flange to shell weld discussed here. However, extensive validation of the computational weld model is available in the main body of the report for weld temperature predictions versus time, distortion predictions, and weld residual stresses so that predictions are presented here with confidence in their accuracy.

A large number of weld sequences, weld parameters, and weld geometries were investigated. Each weld pass is modeled by using a moving heat source as the weld is deposited. A ten-degree segment was modeled with appropriate boundary conditions. The final sequence suggested by the NESC team is shown in the upper left inset (above). It is seen that a 7 pass balanced weld sequence with **the final pass deposited on the OD is the optimum** since it induces compressive axial residual stresses on the ID at the toe of the weld (above). The location at the toe of the fillet at the mouse-hole location (lower left inset) was determined to be the critical CIFS location. Circumferential cracks, driven by axial stresses are the controlling crack growth situation here since they combine unfavorably with service loads.

Some key results from the computational weld assessment are listed here.

- Computational weld models are effective tools to control weld residual stresses, distortions, and microstructure in welds.
- The weld sequence should be properly designed to induce residual stresses at locations and magnitudes to reduce residual stresses and constraint.
- For the Ares I-X weld, a balanced double-vee joint with the final pass on the shell OD is preferred. This not only improves fatigue performance and increases the CIFS, but also will help prevent corrosion.
- The weld joint for the Ares I-X, along with the weld parameters produces high constraint in the joint. High constraint can reduce fracture toughness.
- A weld fixture could be designed using the computational weld tools to minimize distortion of the ring flange. This could reduce fit up stresses during bolt tightening of the flanges during assembly.

References

1. User Manual for VFT – Virtual Fabrication and Weld Modeling Software by Battelle Memorial Institute and Caterpillar Inc., February 2005.

2. Oh, J., and Brust, F. W., “Phase Transformation Effects on Weld Distortion and Residual Stress Predictions”, in Proceedings of PVP2005, 2005 ASME Pressure Vessels and Piping Division Conference, July 17-21, 2005, Denver, Colorado USA, In *Welding and Residual Stresses,* edited by O’Dowd, N., Brust, F. W., Keim, E., Sherry, A., and Dong, P.
3. Brust, F. W., Yang, Y. Y., Ezeilo, A., and McPherson, N., “Weld Modeling of Thin Structures With VFT”, Proceedings of ASME Pressure Vessel and Piping Conference, San Diego, CA, July 2004, in *Residual Stress, Fracture, and Stress Corrosion Cracking,* Principal Editor, Y. Y. Wang, 2004.
4. Chen, X. L., Yang, Z, and Brust, F. W., “Modeling Distortion and Residual Stress During Welding”, Chapter 7 in *Processes and Mechanisms of Welding Residual Stress and Distortion,* pp. 225 – 263, Woodhead Publishing, July 2005.
5. Brust, F. W., and Kim, D., “Mitigating Welding Residual Stress and Distortion”, Chapter 8 in *Processes and Mechanisms of Welding Residual Stress and Distortion,* pp. 264 – 294, Woodhead Publishing, July 2005.
6. Brust, F. W., and Scott, P. M., “Weld Residual Stresses and Primary Water Stress Corrosion Cracking in Bimetal Nuclear Pipe Welds”, PVP 2007-26297, Proceedings of the ASME PVP 2007/Creep 8 Conference, ASME, July 22-26, 2007, San Antonio, Texas, USA.
7. Scott, P. M., Brust, F. W., et al, “The Battelle Integrity of Nuclear Piping (BINP) Final Report”, Nuclear Regulatory Commission Report NUREG/CR-6837, Vol. 1 and 2, Prepared by Battelle and Engineering Mechanics Corp., June 2005.
8. Feng, Z., (Editor), “Processes and Mechanisms of Welding Residual Stress and Distortion” Woodhead Publishing Company, Cambridge, UK, 2005.
9. Cao, Z. Brust, F. W., Nanjundan, A., Dong, Y., and Jutla, T., “A Comprehensive Thermal Solution Procedure for Different Weld Joints”, Advances in Computational Engineering and Sciences; ed. S. N. Atluri and F. W. Brust, Tech Science Press, pp 630-636, August 2000.
10. Brust, F. W., Jutla, T., Yang, Y., Cao, Z., Dong, Y., Nanjundan, A., Chen, X. L., Advances in Computational Engineering and Sciences; ed. S. N. Atluri and F. W. Brust, Tech Science Press, pp 630-636, August 2000. Also, Numerous Weld Papers in this set of volumes on Weld modeling by these authors.
11. Rosenthal, D., “Mathematical Theory of Heat Distributions During Welding and Cutting,” *Welding Research Journal Supplement,* May 1941, pp. 220-234.
12. Rybicki, E. F., Schmueser, D. W., Stonesifer, R. B., Groom, J. J., and Mishler, H. W., "A Finite Element Model for Residual Stresses and Deflections in Girth-Butt Welded Pipes," Journal of Pressure Vessel Technology, Vol. 100, pp. 256-262, August 1978.
13. Rybicki, E. F., and Stonesifer, R. B., "Computation of Residual Stresses Due to Multipass Welds in Piping Systems," Journal of Pressure Vessel Technology, Vol. 101, pp. 149-154, May 1979.

14. Bagshaw, N., and Mawella, J., "Prediction and Control of Distortion During Welding Ship Panesl", Proc. 2007 CF/DRDC International Defense Applications of Materials Meeting in Halifax, NS, Canada, 5-7 June 2007.

15. Withers, P. J., "Residual Stress and its Role in Failure", Reports on Progress in Physics, Volume 70, pp 2211-2264, 2007.

16. Turski, M., Edwards, L., James, J., Bouchard, P. J., Smith, M., and Withers, P. J., "Residual Stress Measurement Within A Single Pass Grove Weld Specimen Utilizing Neutron Diffraction and the Contour Method" , 2006 ASME Pressure Vessel and Piping Conference, Vancouver, BC, Canada, PVP2006-ICPVT-11-93991, July, 2006.

17. Taylor, N. G., Faidy, C., and Gilles, P. (Editors), *Assessment of Dissimilar Weld Integrity: Final Report to the NESC-III Project,* European Commission Report (EUR 22510 EN), Luxembourg, 2006.

18. Brust, F. W., and Scott, P. M., "Weld Residual Stresses and Primary Water Stress Corrosion Cracking in Bimetal Nuclear Pipe Welds", Proceedings of the ASME PVP 2007/Creep 8 Conference, July 22 – 26, San Antonio, Texas, Paper PVP 2007-26297, 2007.

19. Brust, F. W., and Scott, P. M., "Primary Water Stress Corrosion Cracking (PWSCC) in Bimetal Nuclear Pipe Welds – Analysis Considerations", Proc. 19th International Conference on Structural Mechanics in Reactor Technology (SMiRT 19), August 12-17, Toronto, Canada, 2007.

20. Knight, N. F., Jr., Phillips, D. R., and Raju, I. S., *Ares I-X Upper Stage Simulator Structural Analyses Supporting the NESC Critical Initial Flaw Size Assessment*, NASA TM-2008-215336, 2008.

21. D. S. Dawicke, I. S. Raju, and D. Cheston "Ares I-X USS Critical Initial Flaw Size Analysis", NASA TM-215337, January 2008.

22. Cheston, D., et al, "Independent Evaluation of the Critical Initial Flaw Size for the Ares 1-X (AIX) Upper Stage Simulator (USS) Common Segment Flange-to-Skin Welds", NASA TM-215351, 2008.

23. Brust, F. W., and Scott, P. M., "Weld Distortion Control Methods and Applications of Weld Modeling", Proc. 19th International Conference on Structural Mechanics in Reactor Technology (SMiRT 19), August 12-17, Toronto, Canada, 2007.

24. Scott, P. M., Brust, F. W., et al, "The Battelle Integrity of Nuclear Piping (BINP) Final Report", Nuclear Regulatory Commission Report NUREG/CR-6837, Vol. 1 and 2, Prepared by Battelle and Engineering Mechanics Corp., June 2005.

25. Rybicki, E. F., McGuire, P. A., Stonesifer, R. B., and Brust, F. W., "Applications of Computational Models for Controlling Weld Residual Stresses in BWR Piping", Seminar on Countermeasures for BWR Pipe Cracking, EPRI Session 3, January 22-24, 1980.

26. F. W. Brust and E. F. Rybicki, "Computational Model of Backlay Welding for Controlling Residual Stresses in Welded Pipes," in Journal of Pressure Vessel Technology - Trans. ASME, Vol. 103, August, 1981, pp. 294-299.

27. Brust, F. W., and Dong, P., “Welding Residual Stresses and Effects on Fracture in Pressure Vessel and Piping Components: A Millennium Review and Beyond”, Transactions of ASME, Journal Of Pressure Vessel Technology, Volume 122, No. 3, August 2000, pp329-339.

28. Rybicki, E. F., McGuire, P. A., Merrick, E., and Wert, E., "The Effect of Pipe Thickness on Residual Stresses due to Girth Welds," Journal of Pressure Vessel Technology, Vol. 104, pp. 204-209, August 1982.

29. Fredette, L., and Brust, F. W., ‘Effect of Weld Induced Residual Stresses On Pipe Crack Opening Areas And Implications On Leak-Before-Break Considerations’, ASME Pressure Vessels and Piping Conference, 4-8 August, 2002, Vancouver, British Columbia, Canada. In PVP Volume 434, COMPUTATIONAL WELD MECHANICS, CONSTRAINT, AND WELD FRACTURE, American Society of Engineers (ASME) publication, ed. F. W. Brust, August, 2002.

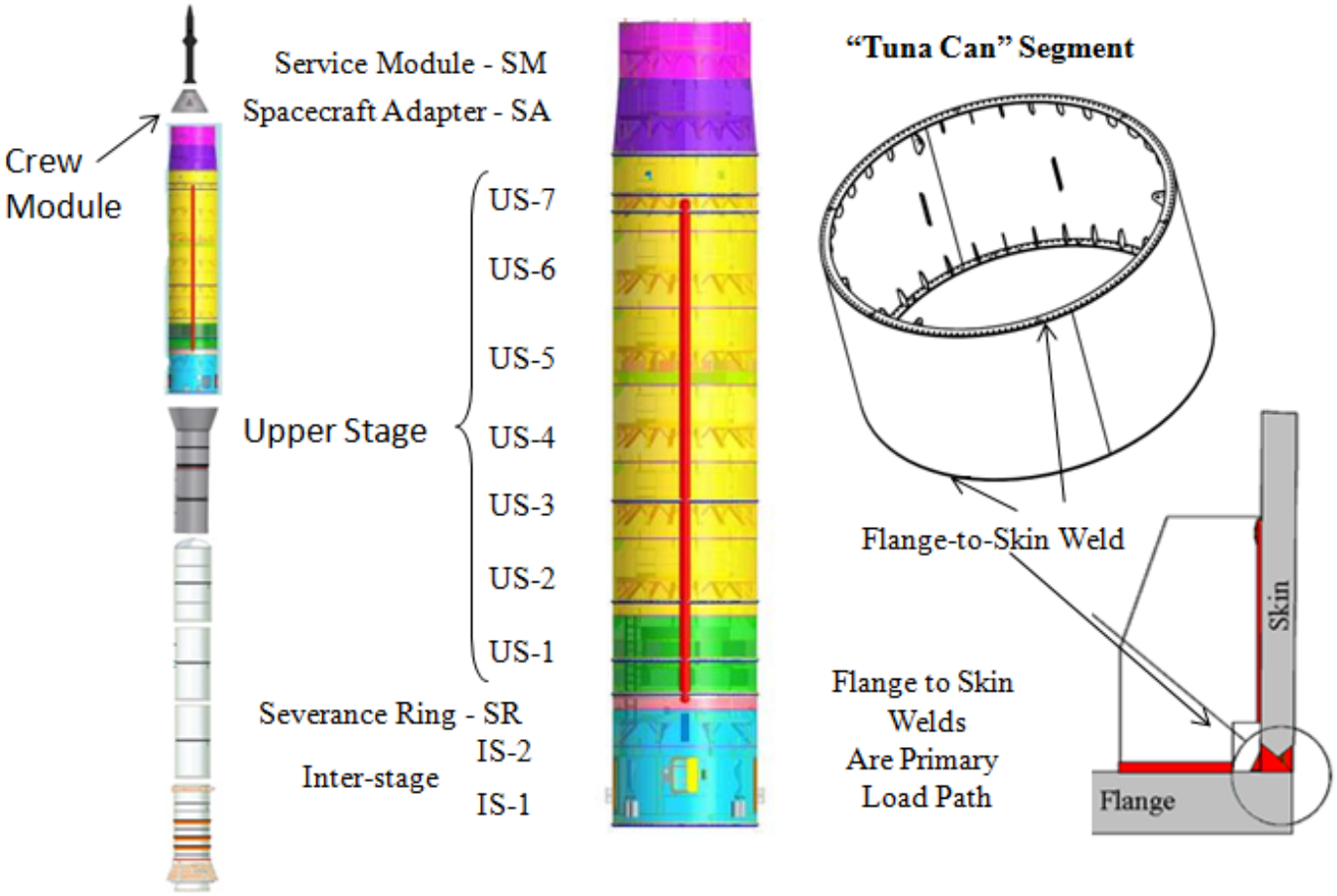

Figure 1. Schematic of the Ares I-X System.

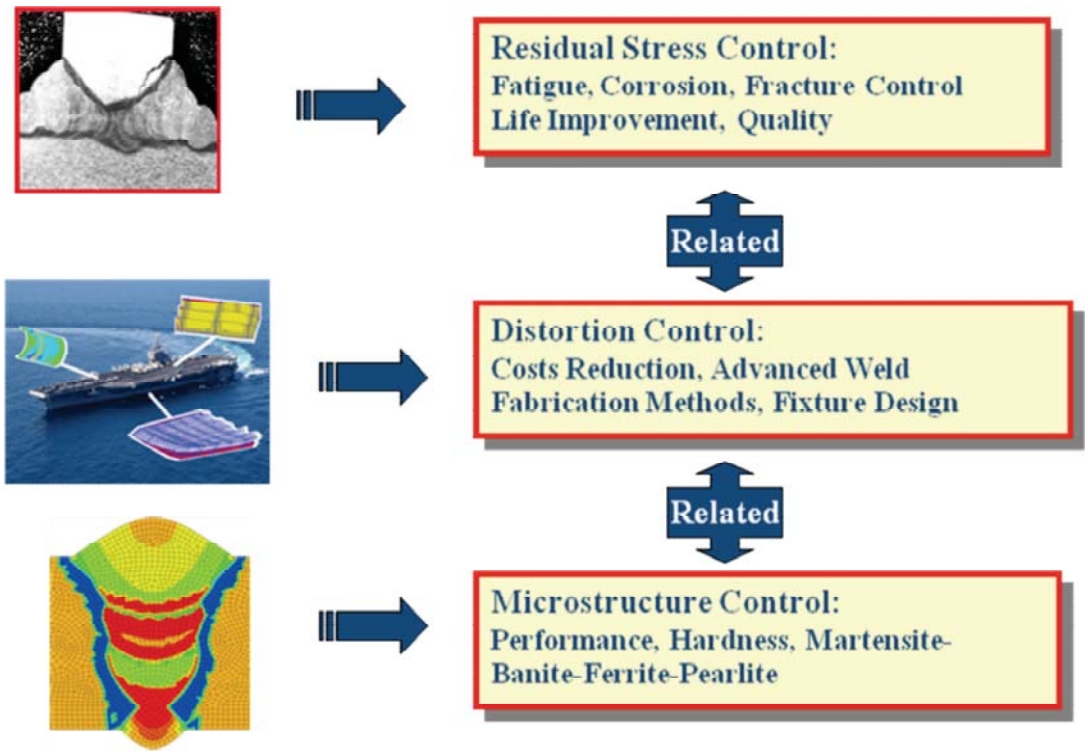

Figure 2. Three benefits of computational weld modeling analysis.

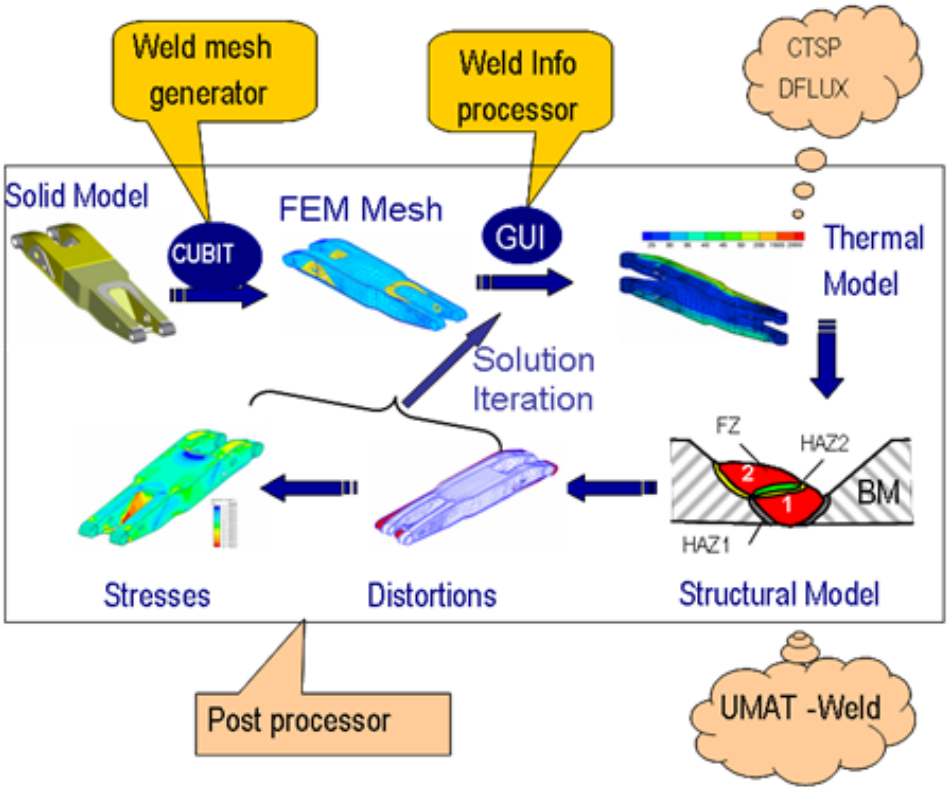

Figure 3. Schematic of weld modeling process used here.

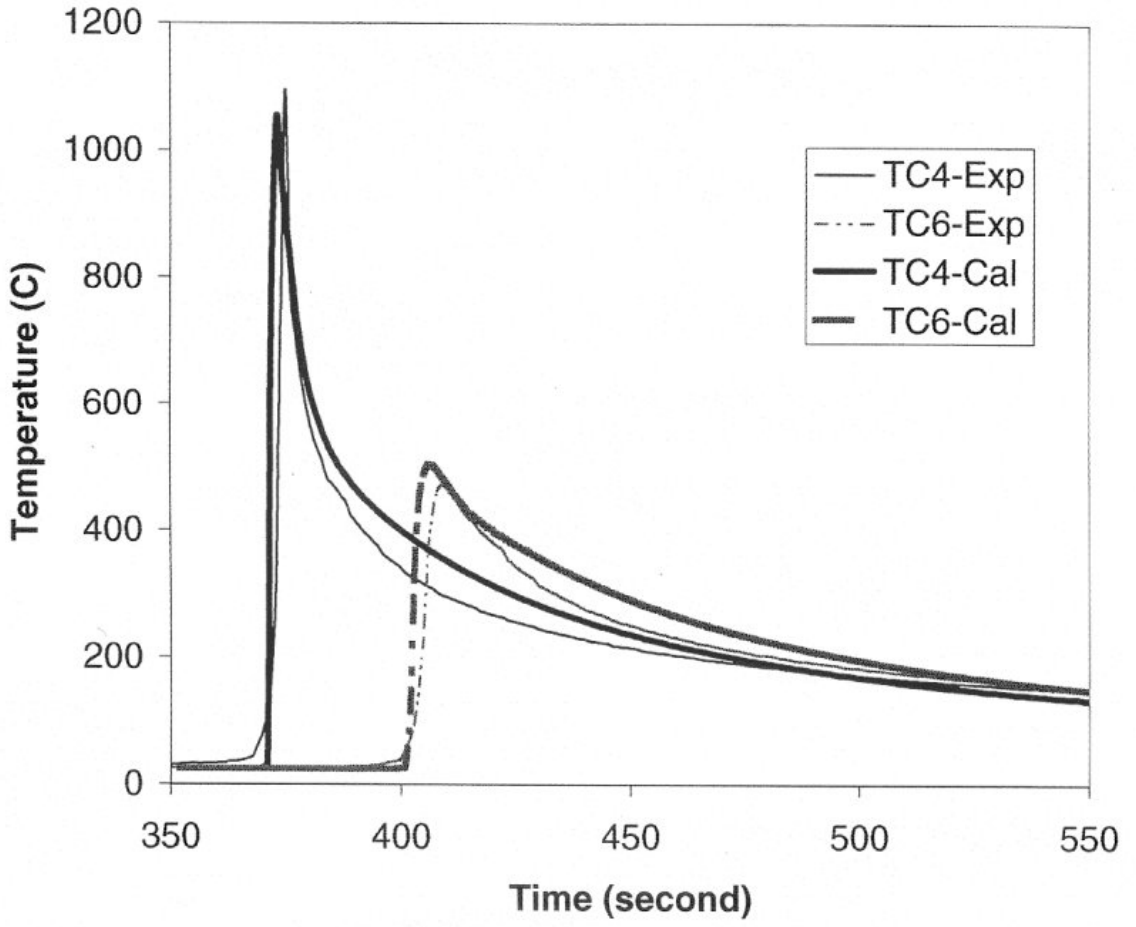

Figure 4. Validation example for CTSP thermal analysis code - Tee fillet weld example.

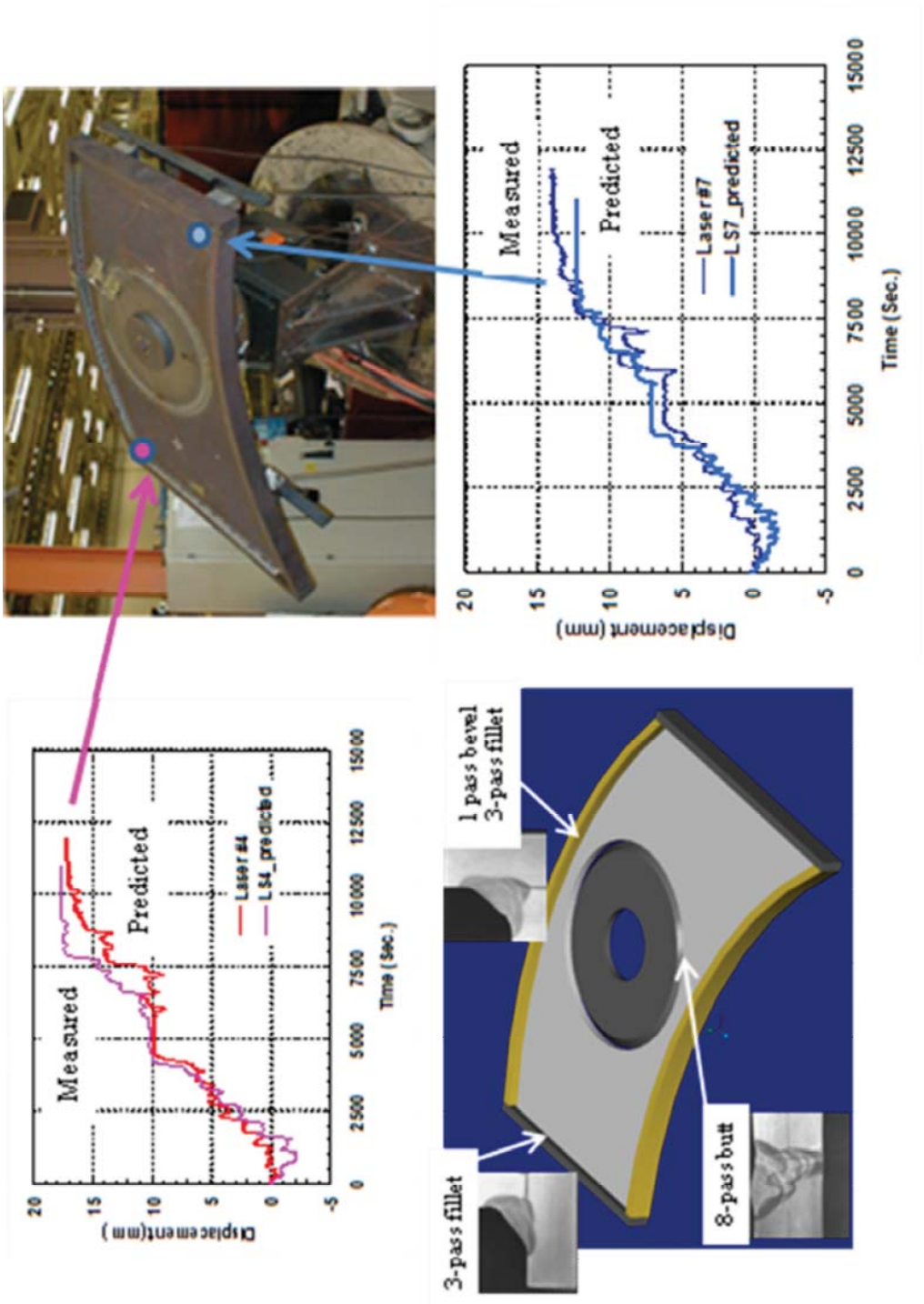

Figure 5. Distortion validation example for distortion prediction of mining equipment.

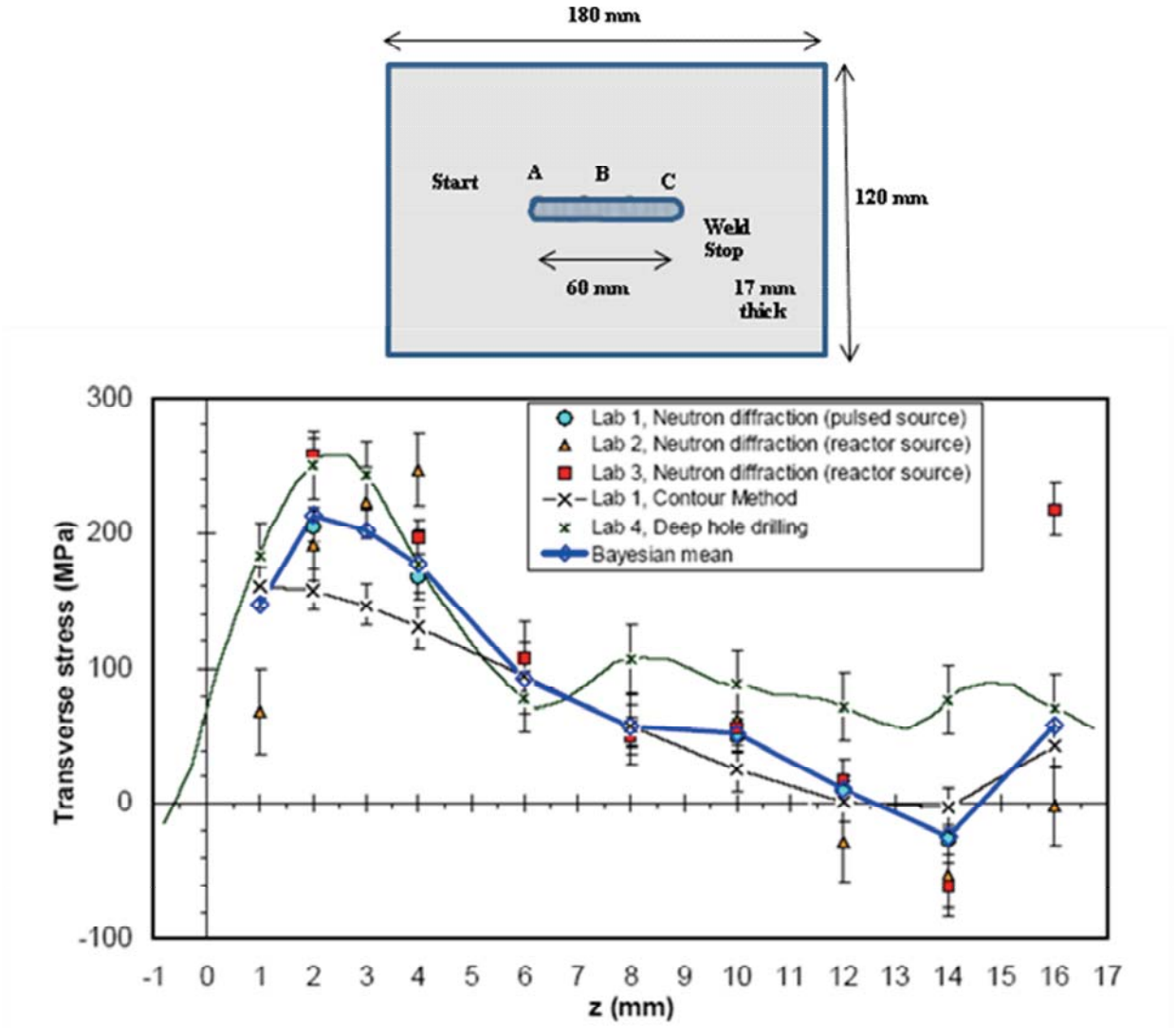

From Reference [12]: Turski, M., Edwards, L., James, J., Bouchard, P. J., Smith, M., and Withers, P. J., "Residual Stress Measurement Within A Single Pass Grove Weld Specimen Utilizing Neutron Diffraction and the Contour Method", 2006 ASME Pressure Vessel and Piping Conference, Vancouver, BC, Canada, PVP2006-ICPVT-11-93991, July, 2006.

Figure 6. Residual stress round robin measurement results. At center of weld through thickness (at 'B').

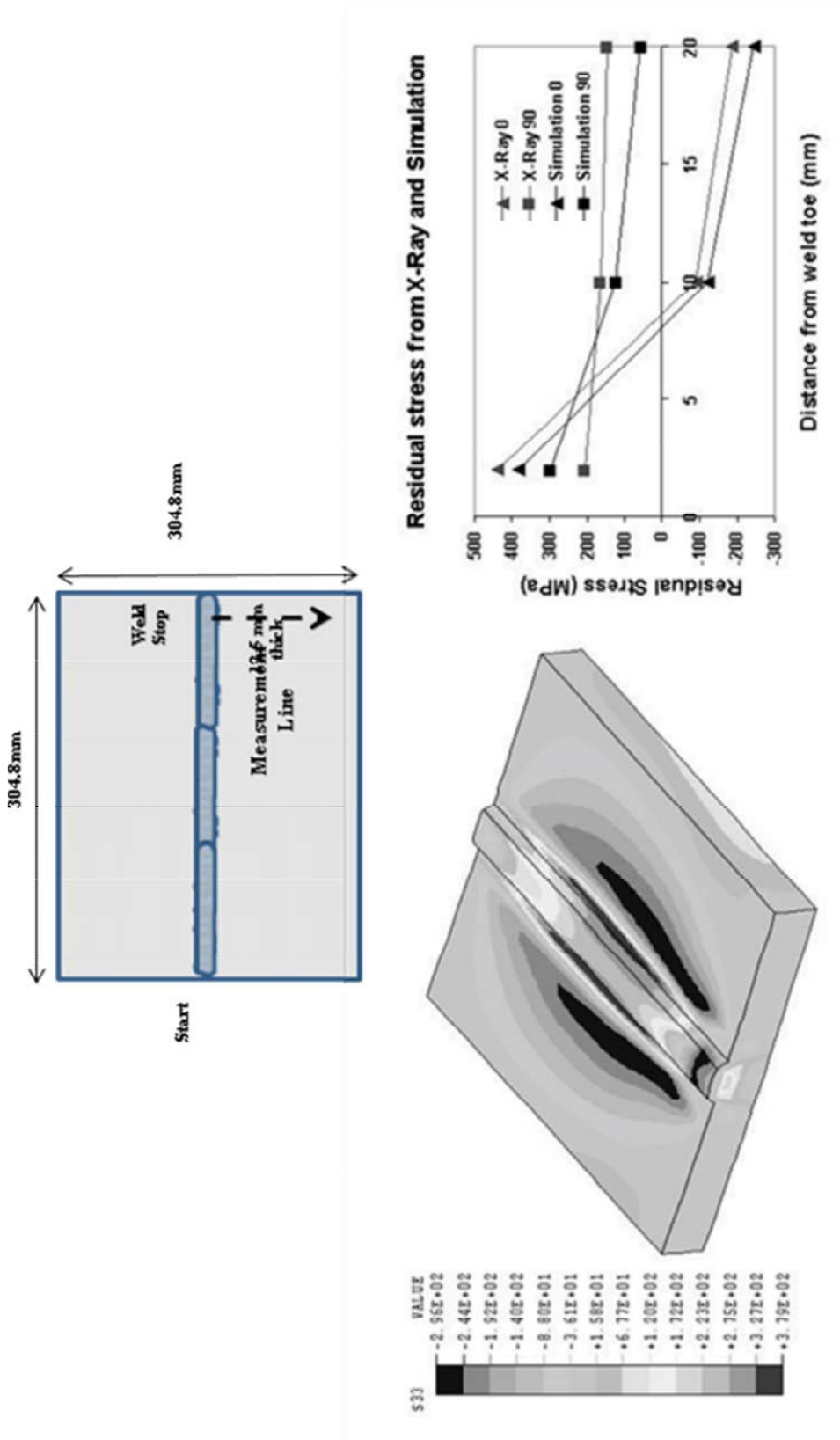

Figure 7. Residual stress round robin measurement results. At center of weld through thickness at 'B'.

Figure 8. NESC bimetal pipe fabrication sequence.

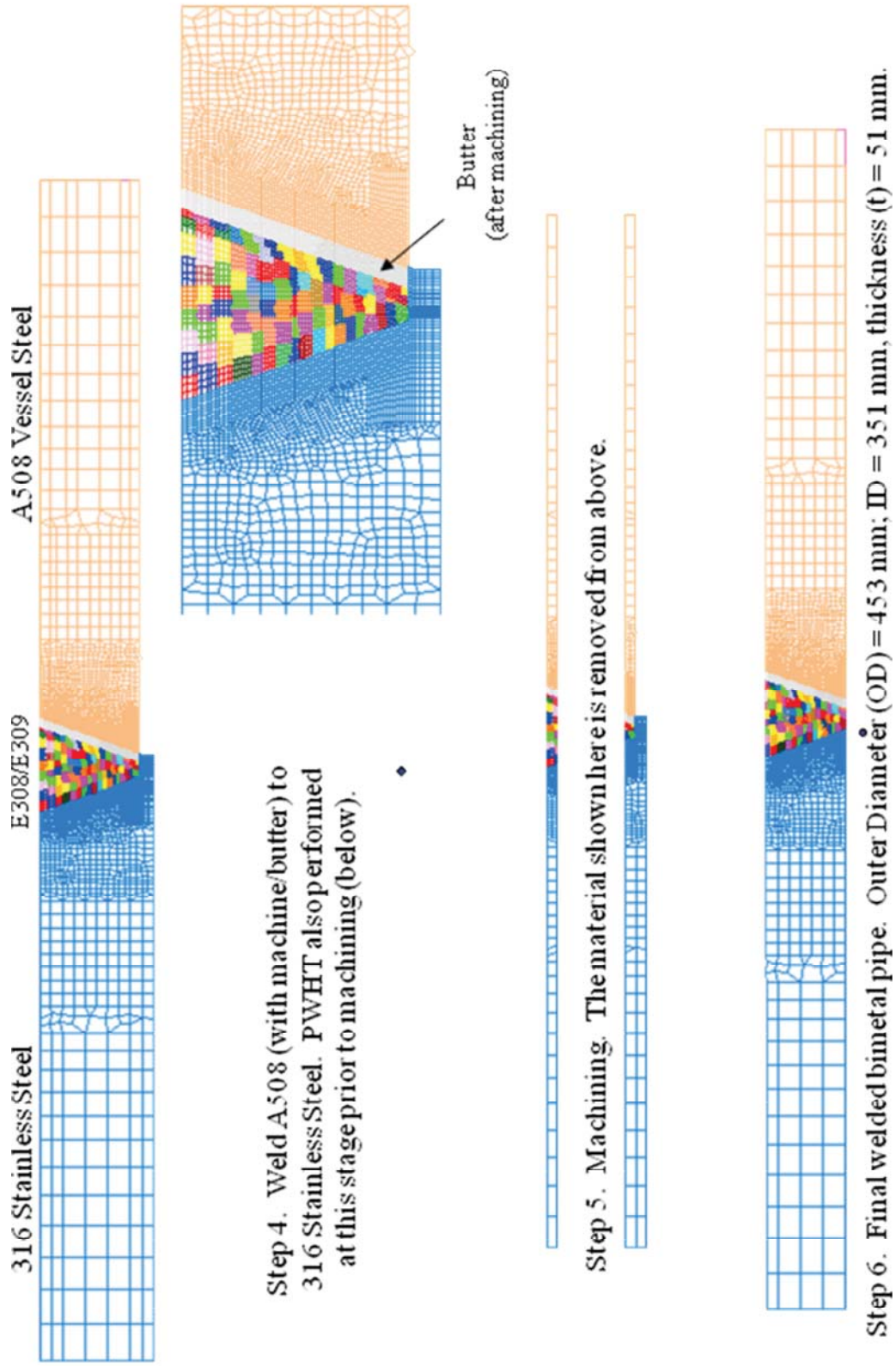

Figure 9. NESC bimetal pipe fabrication sequence (continued).

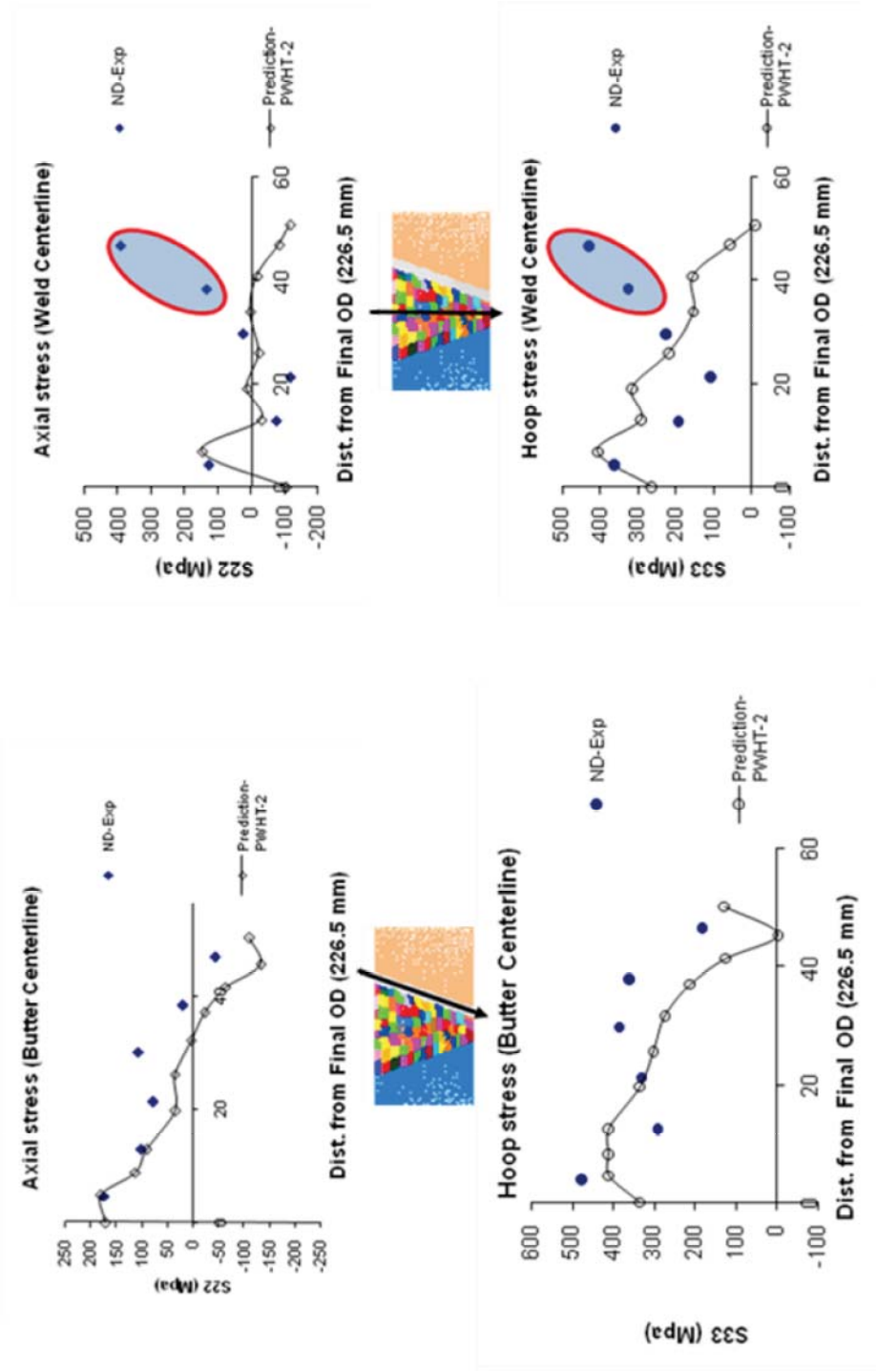

Figure 10 NESC bimetal pipe comparison of neutron diffraction measured residual stresses to model predictions. Thorough butter (left) and through weld centerline (right).

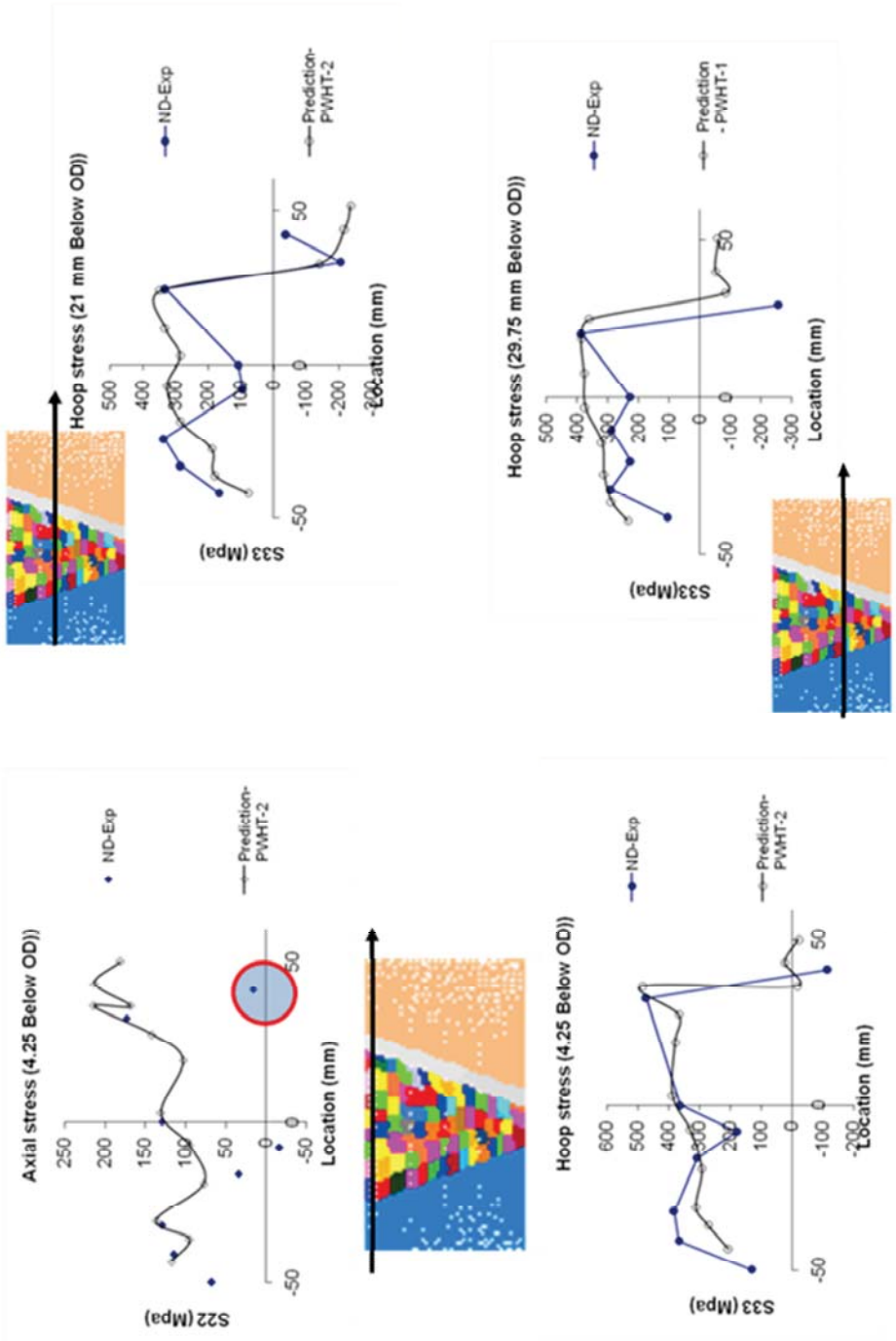

Figure 11. NESC bimetal pipe comparison of neutron diffraction measured residual stresses to weld model predictions. Location - through weld (see inset illustrations).

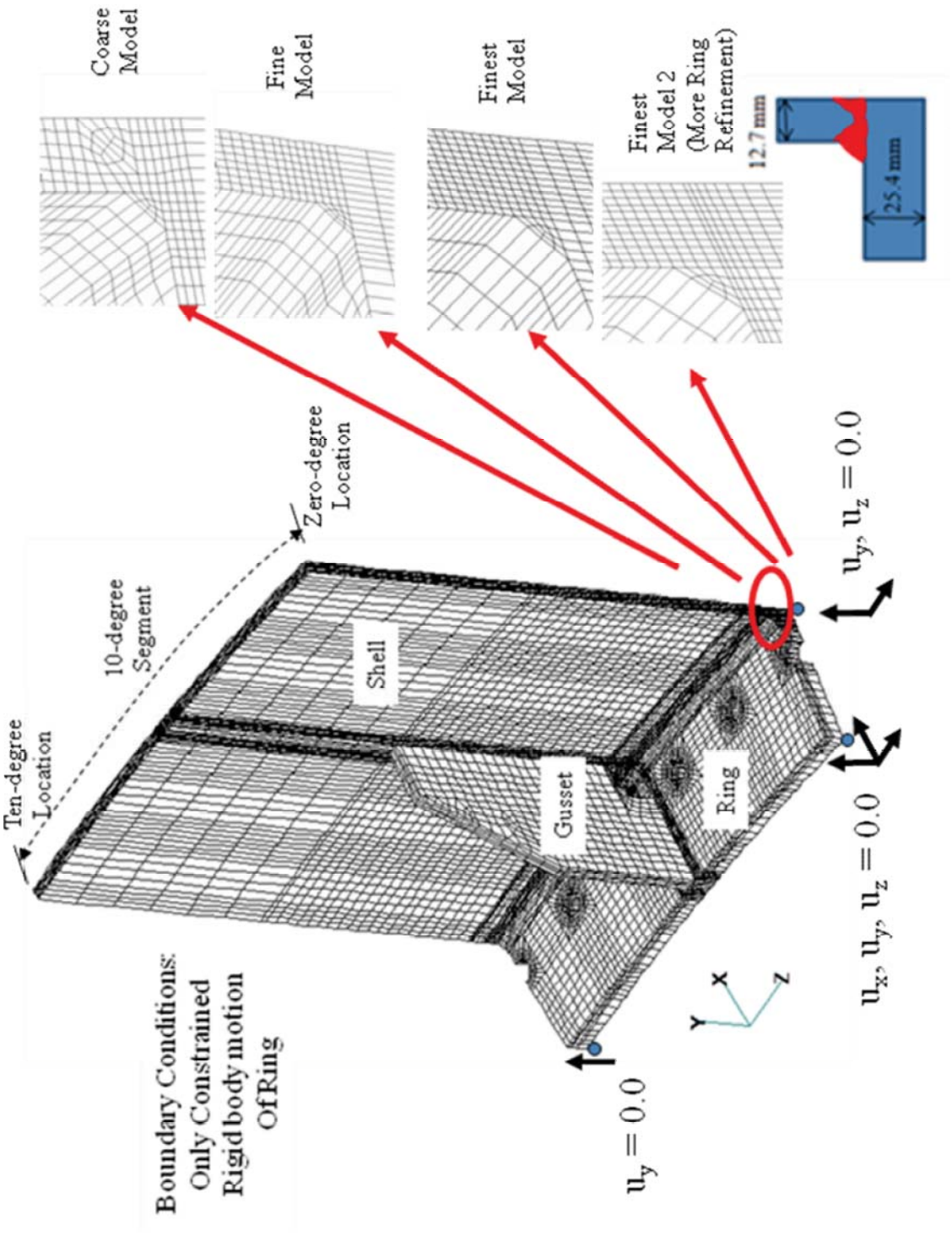

Figure 12. Ten degree segment weld model with four different mesh refinements. The weld joint is seen at the bottom right.

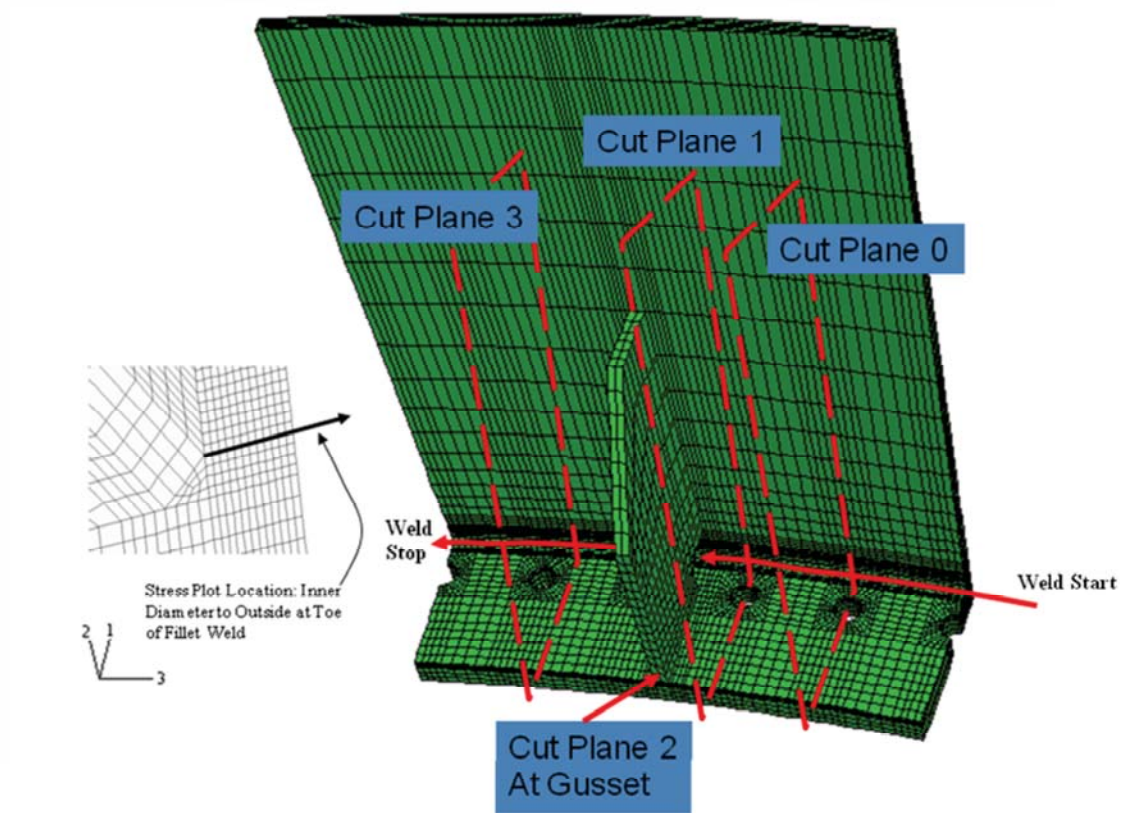

Figure 13. Cut plane definitions. Stresses are plotted at these locations.

Welding Parameters

Pass	Amps	Volts	Weld speed (mm/sec)
1-7	200 - 215	25 - 26	4 -5

Thermal Properties

Specific Heat (J/Kg-C)	Thermal Conductivity (W/mm-C)	Density (Kg/mm^3)
580	0.045	$7.85x10^{-6}$

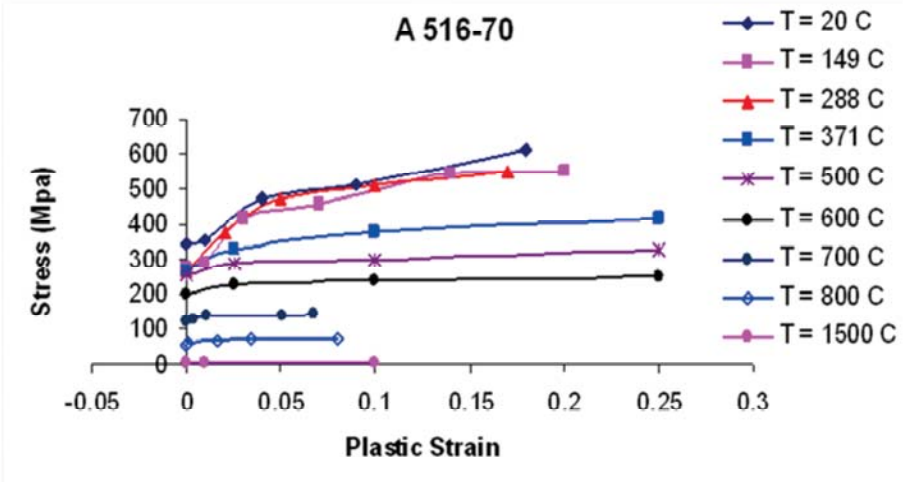

Figure 14. Material properties for A516-70 steel.

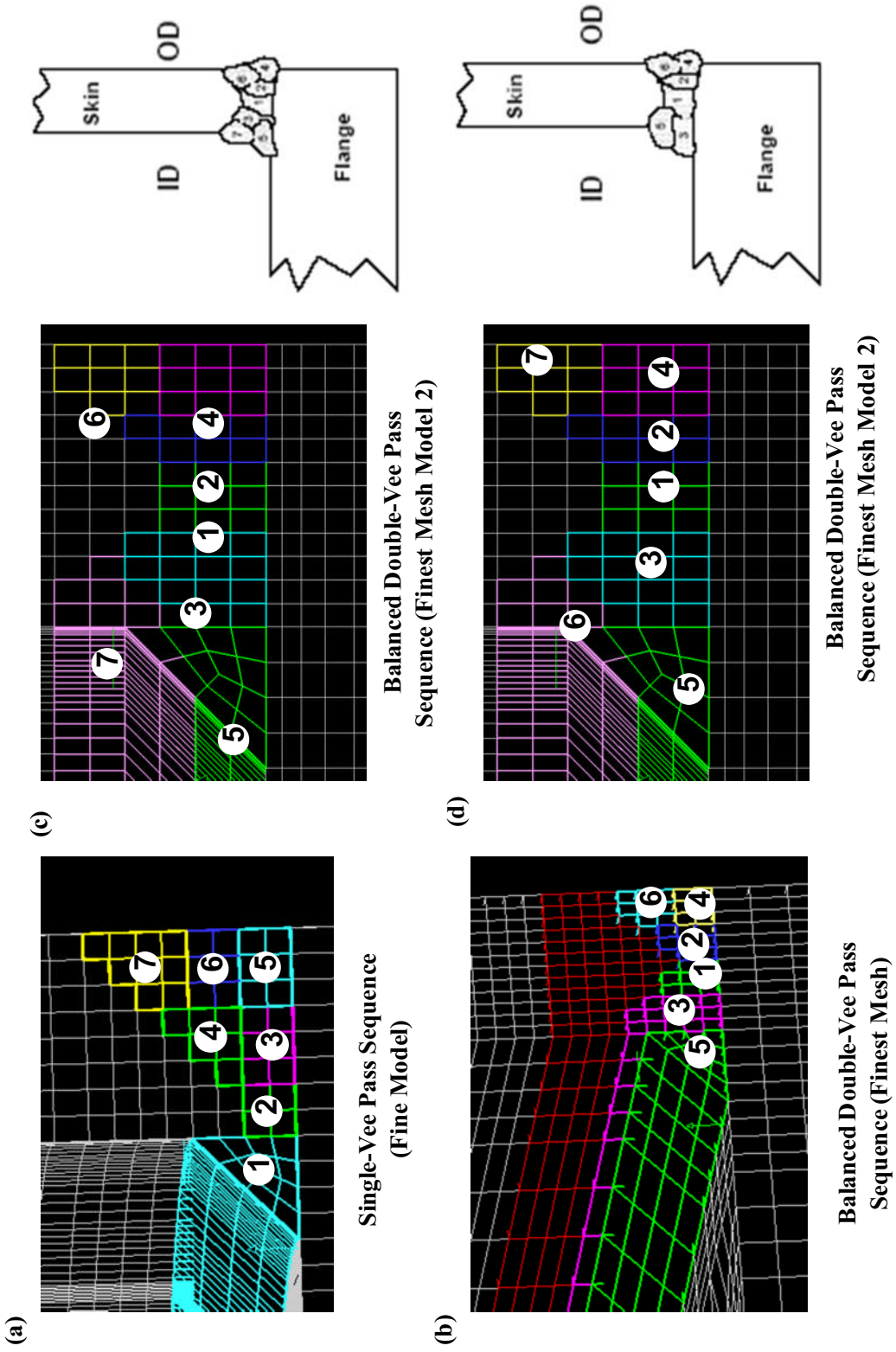

Figure 15. Weld sequences considered.

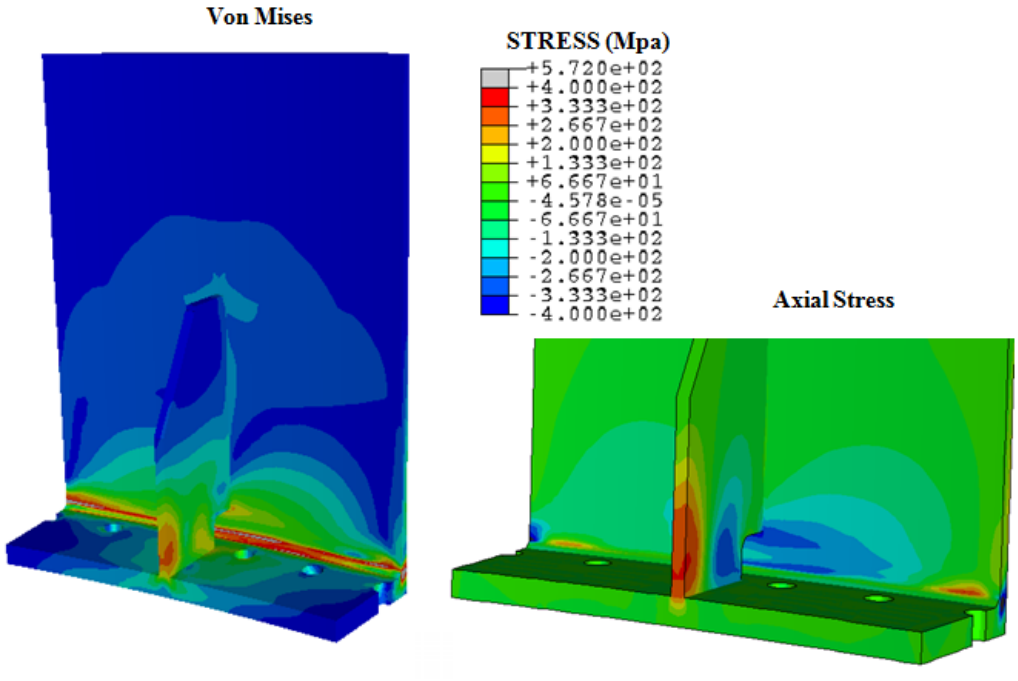

Figure 16. Weld residual stresses for 6-pass case with final pass on the OD (Von Mises and Axial).

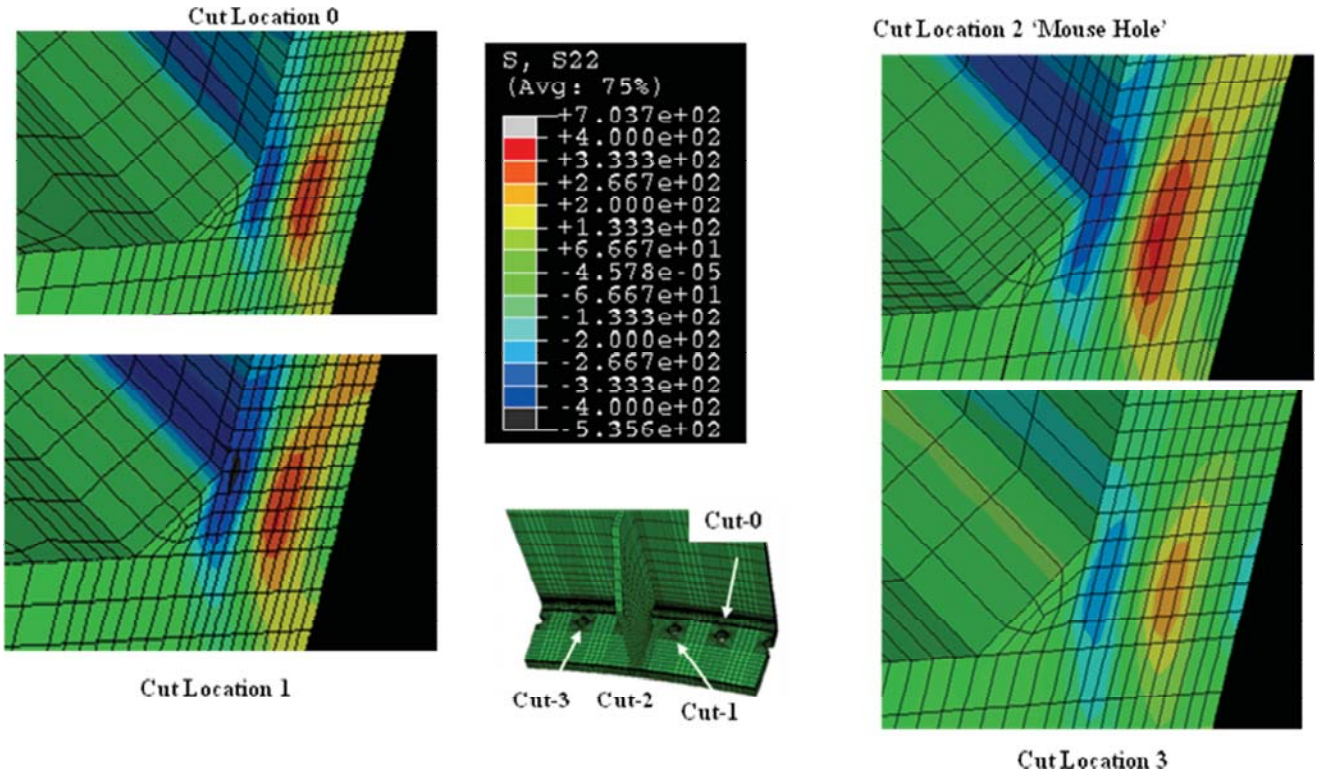

Figure 17. Axial weld residual stresses for double-vee at different locations.

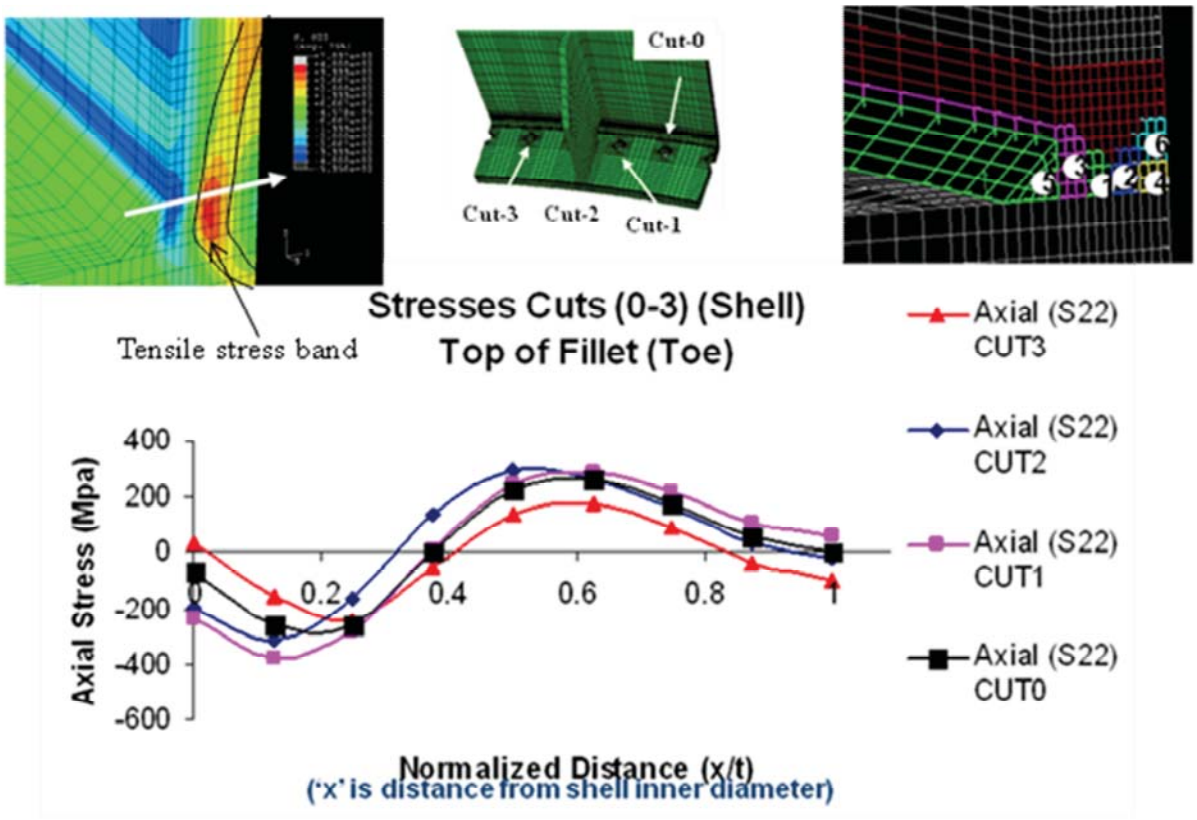

Figure 18. Line plots of axial weld residual stress double-vee, 6-pass weld.

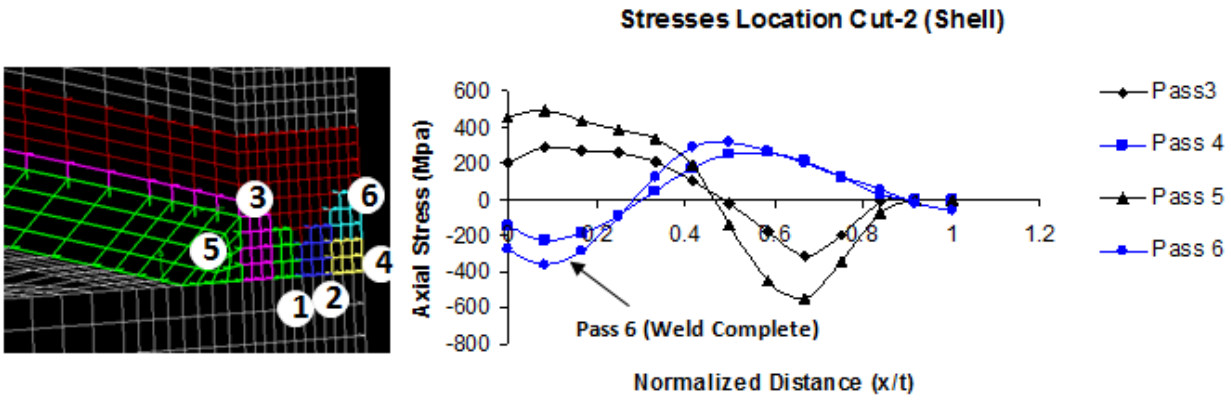

Figure 19. Weld sequence effect on axial stress distribution in Ares I-X 6-pass weld.

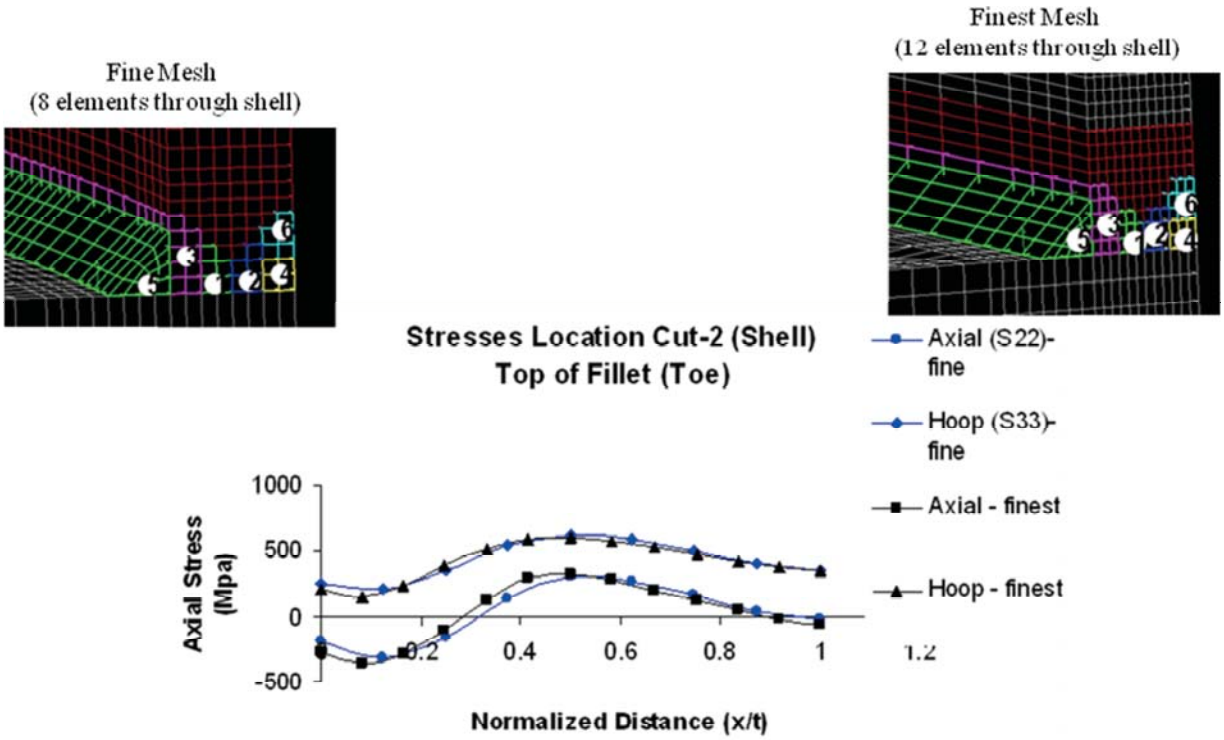

Figure 20. Mesh refinement effect.

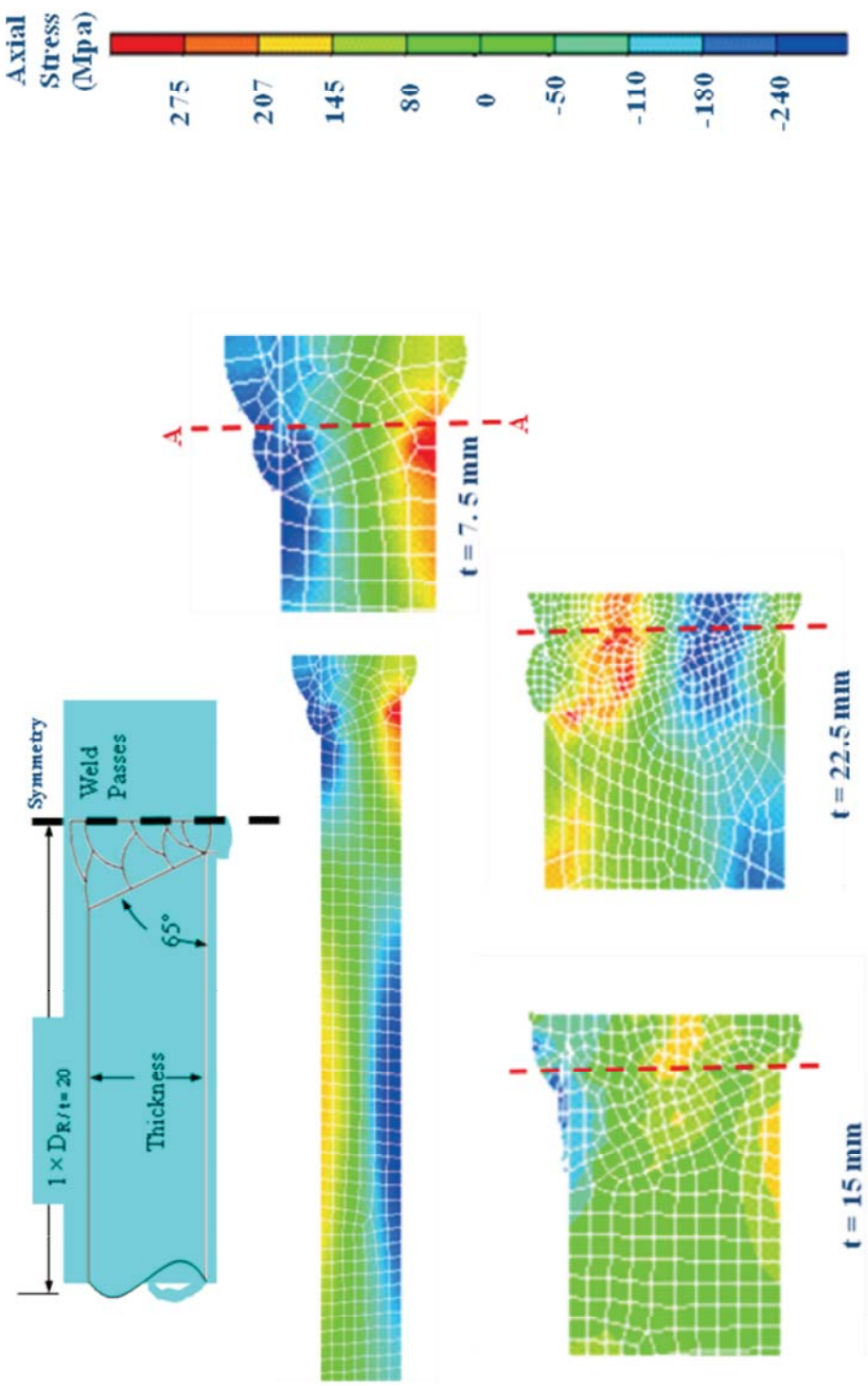

Figure 21. Weld model results for girth welded pipe.

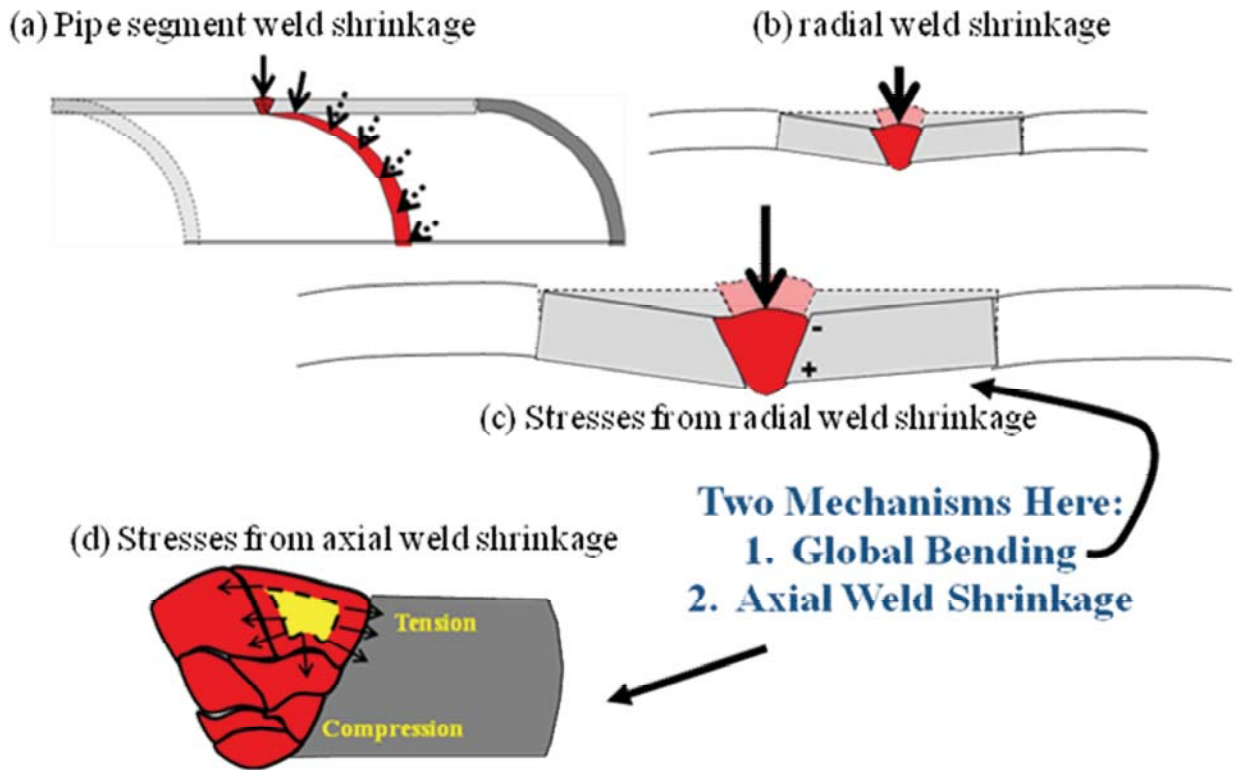

Figure 22. Weld residual stress development in a girth welded pipe. Competing mechanisms between global radial weld bead shrinkage, which induces tension on the pipe ID and compression on the OD (c) and axial shrinkage of the final passes (near pipe OD), causing OD tension and ID compression.

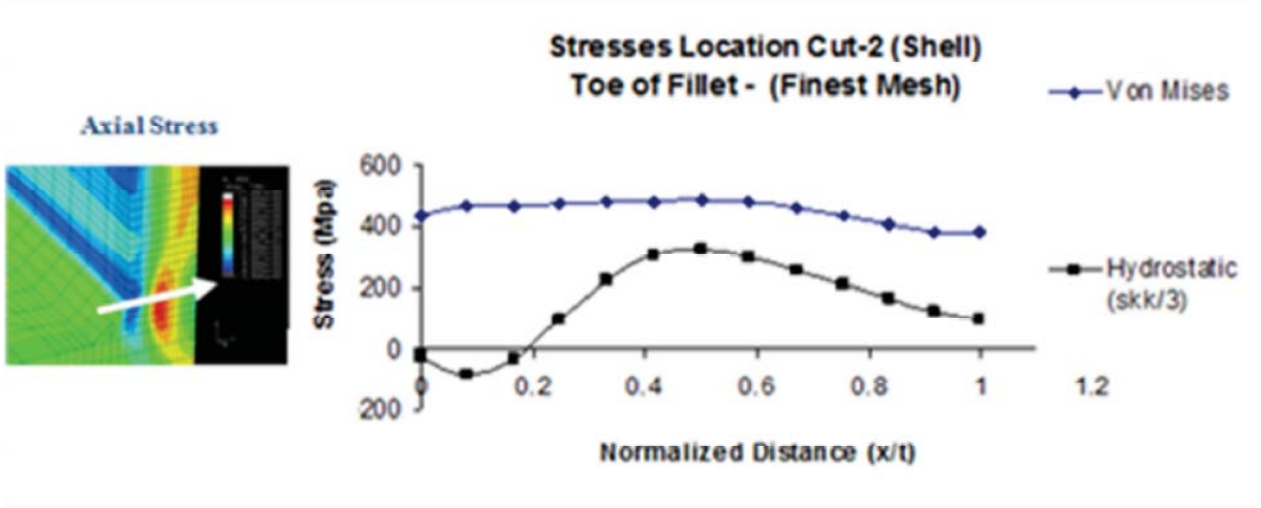

Figure 23. Constraint effects and weld residual stresses.

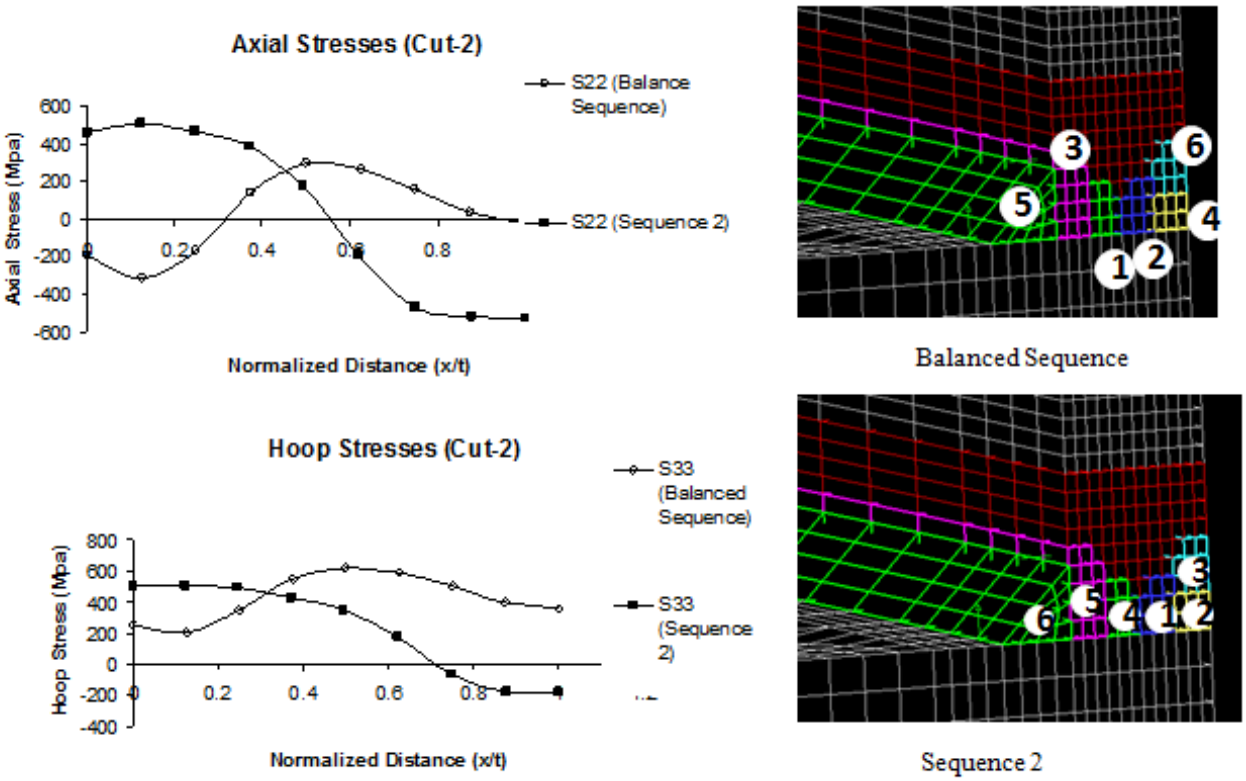

Figure 24. Effect of weld sequence (Cut-2 location).

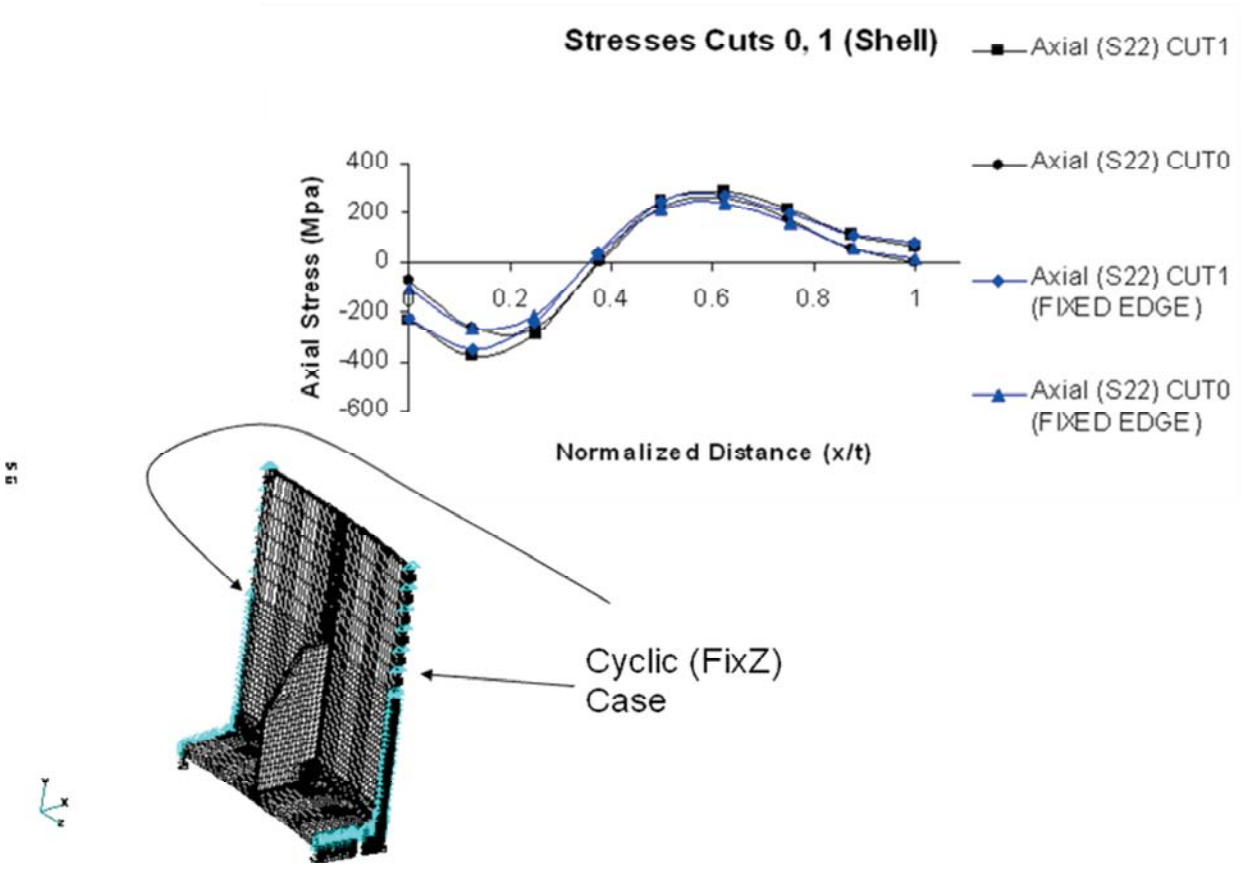

Figure 25. 10-degree segment edge effects and residual stress.

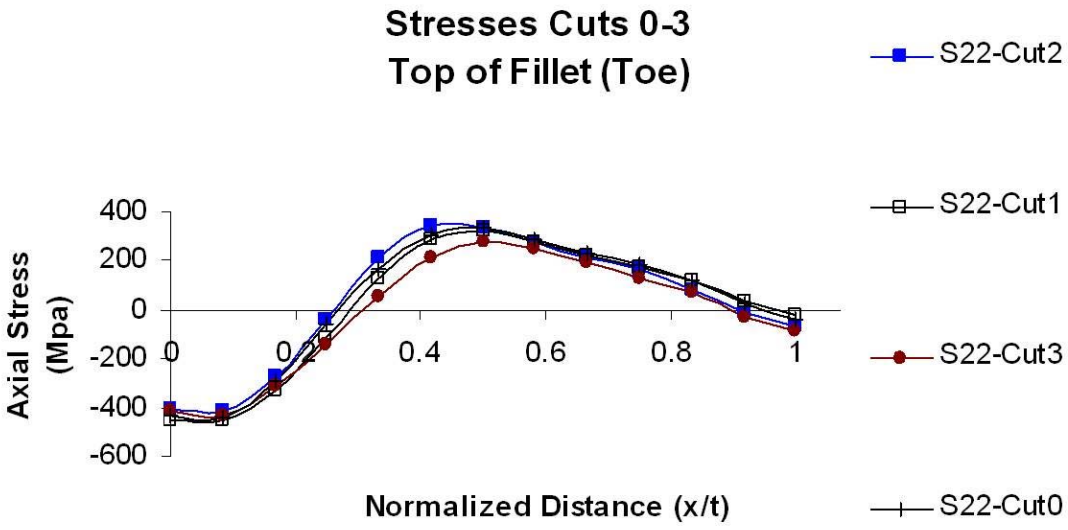

Figure 26. Single-vee axial stress results (finest mesh from Figure 11).

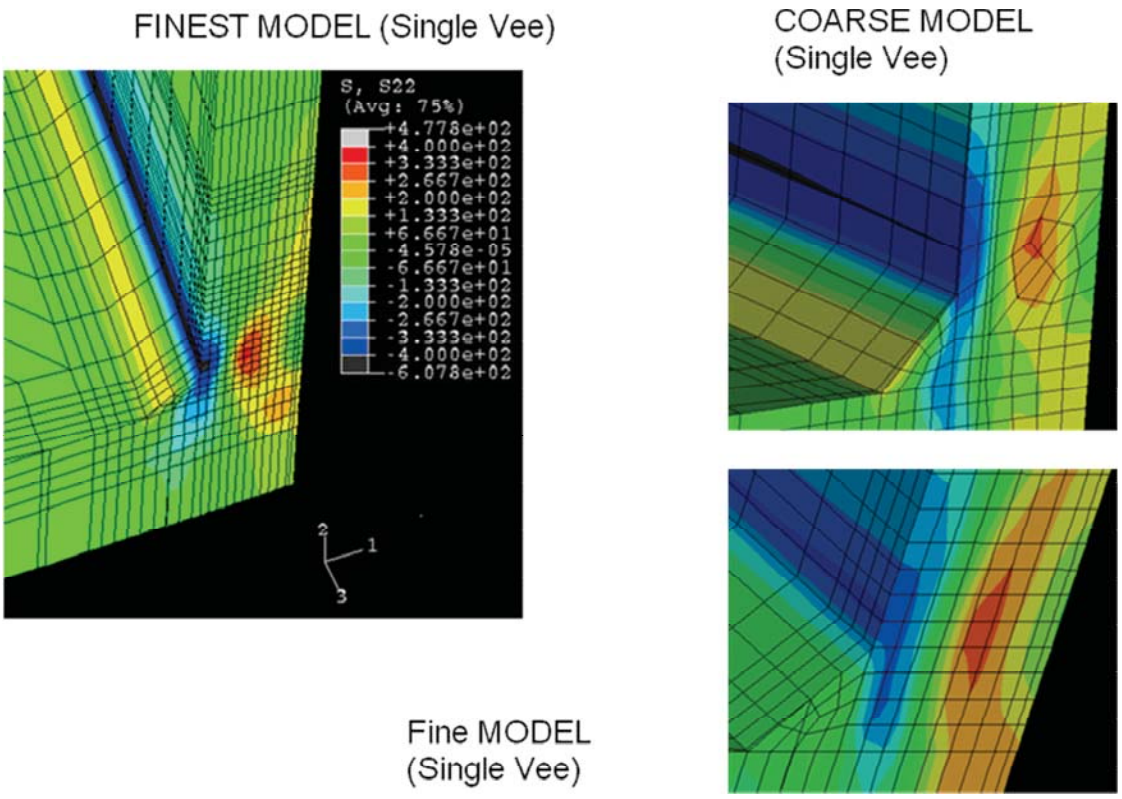

Figure 27. Single-vee axial stress results (7 passes with final pass on OD) at Cut-2 location.

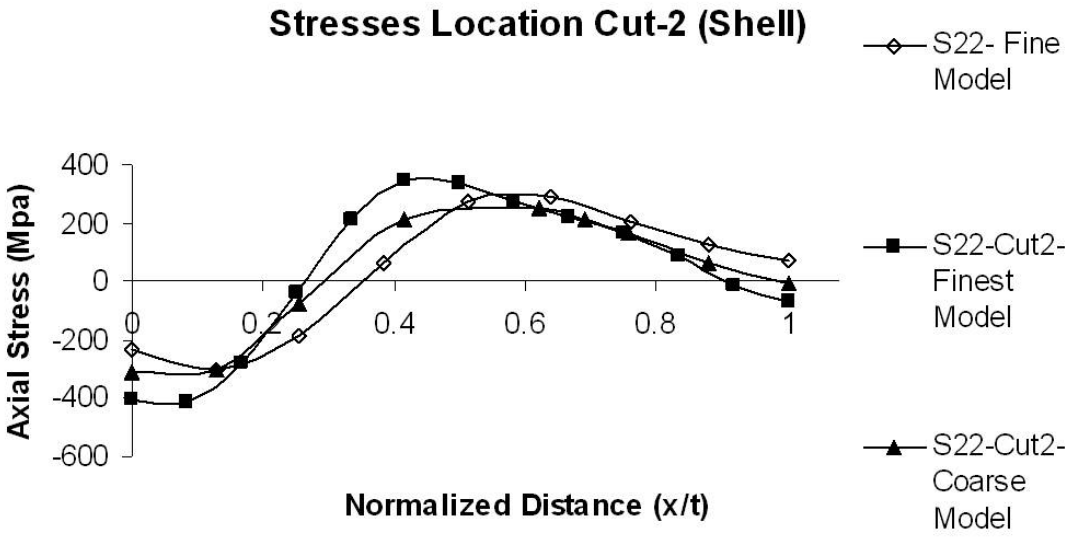

Figure 28. Single-vee axial stress results - mesh sensitivity study.

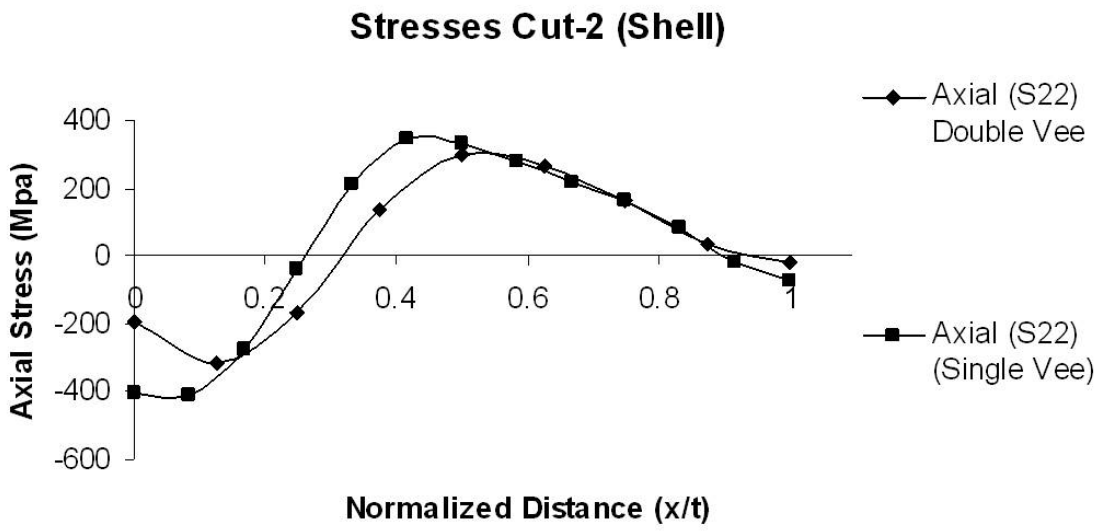

Figure 29. Single-vee axial stress results (finest mesh) compared with double-vee (Cut-2 location).

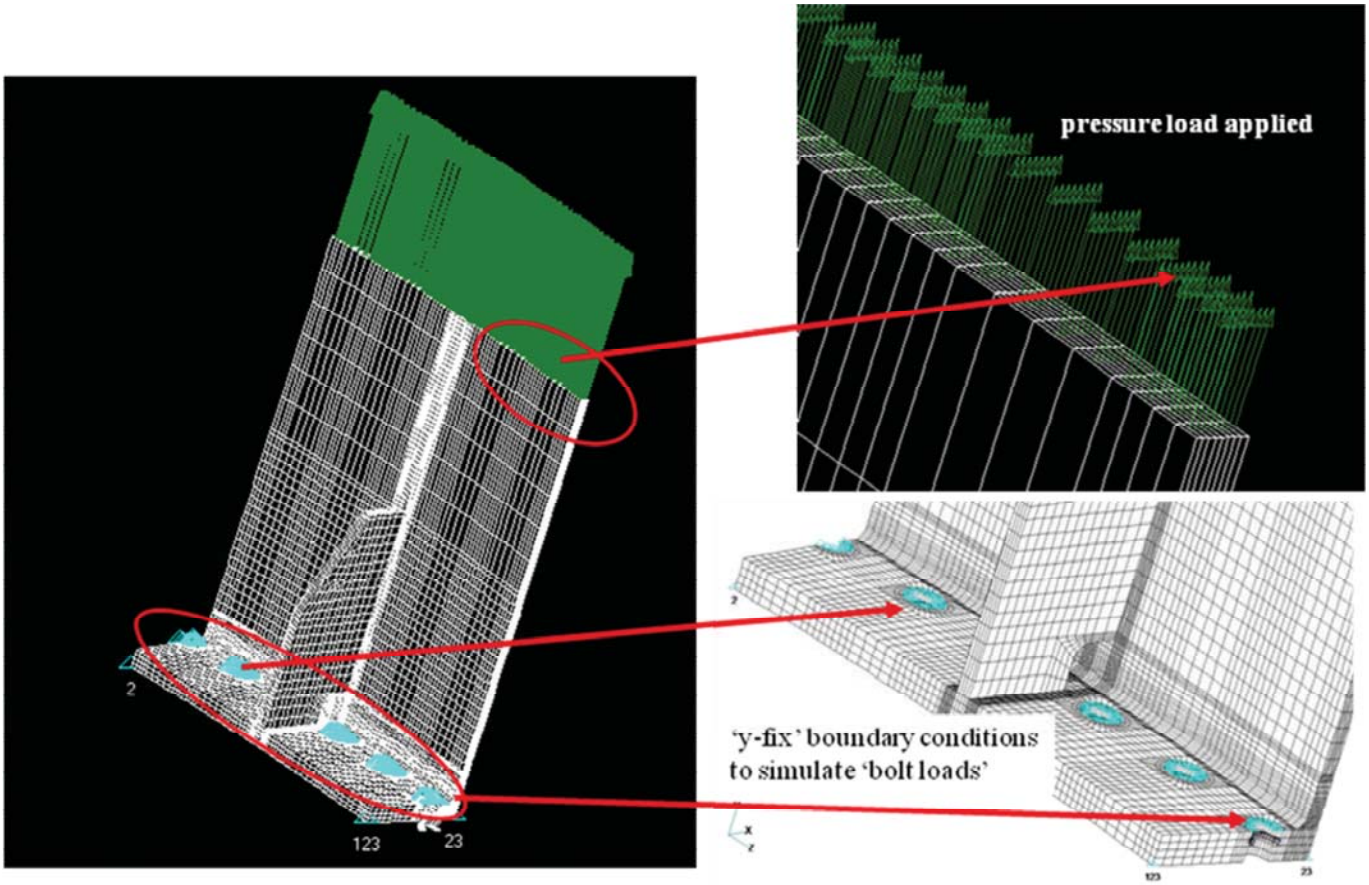

Figure 30. Shakedown loads and boundary conditions.

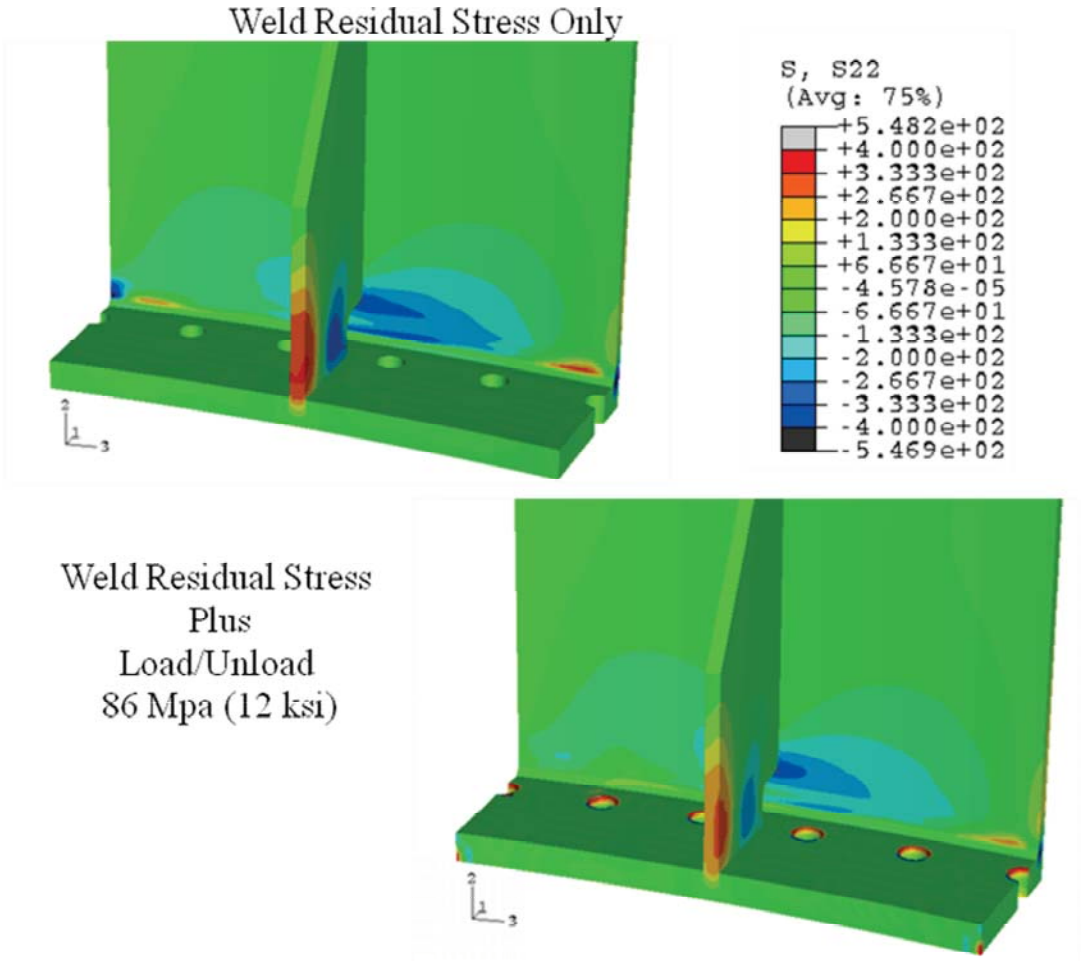

Figure 31. Shakedown stresses after loading and unloading of 86 Mpa.

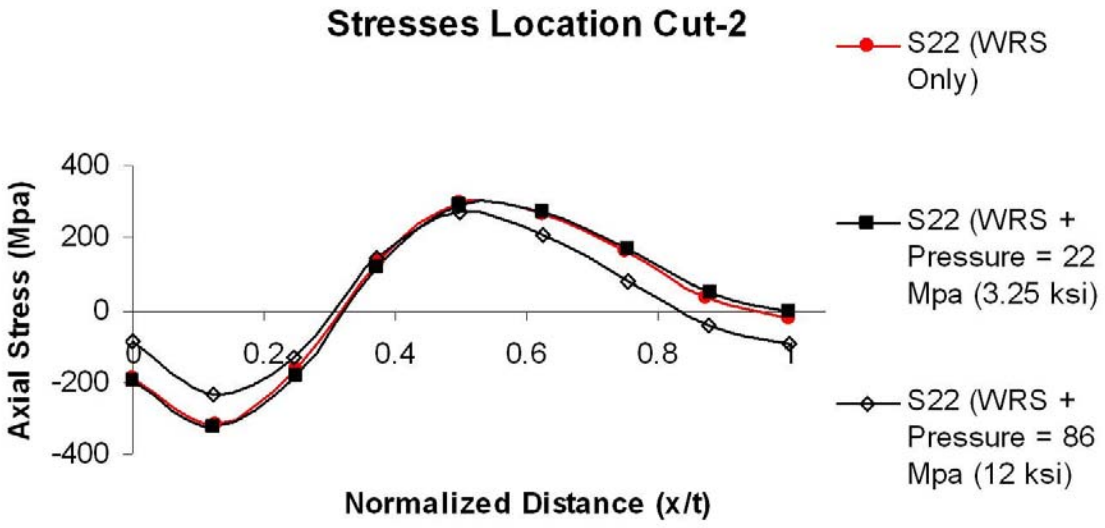

Figure 32. Comparison of axial weld residual stresses after application of pressure and releasing (pressure = 22 and 86 Mpa).

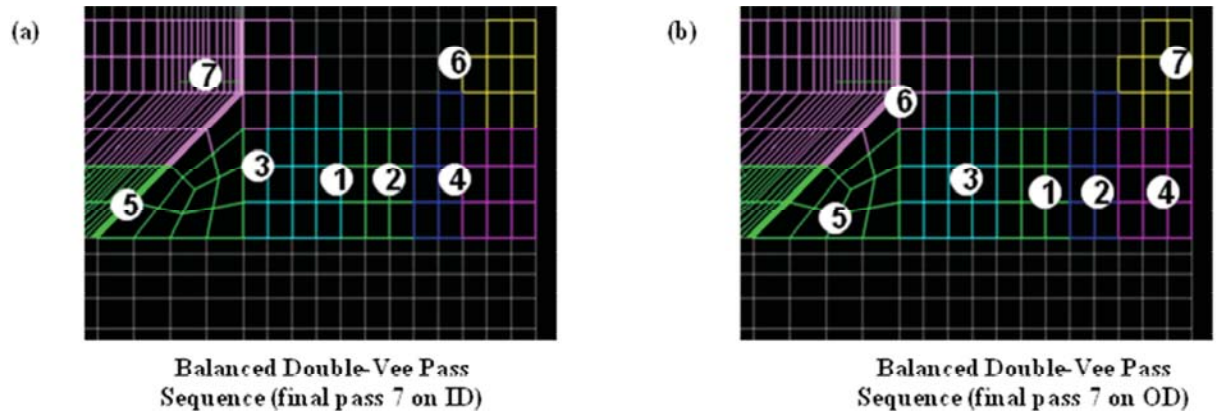

Figure 33. Final model for CIFS study: (a) final pass on ID (b) final pass on OD.

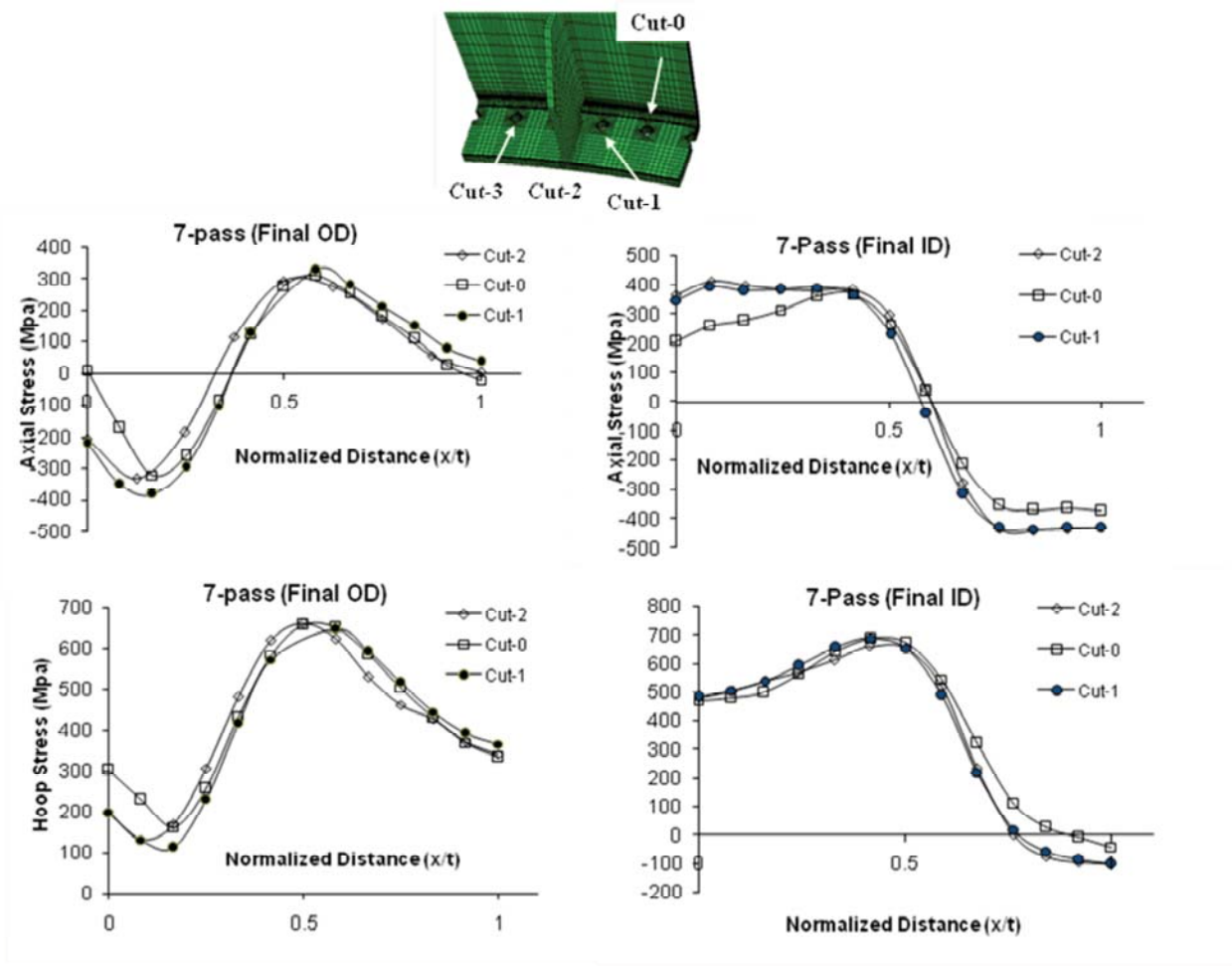

Figure 34. Axial stress line plots at top of fillet weld through shell.

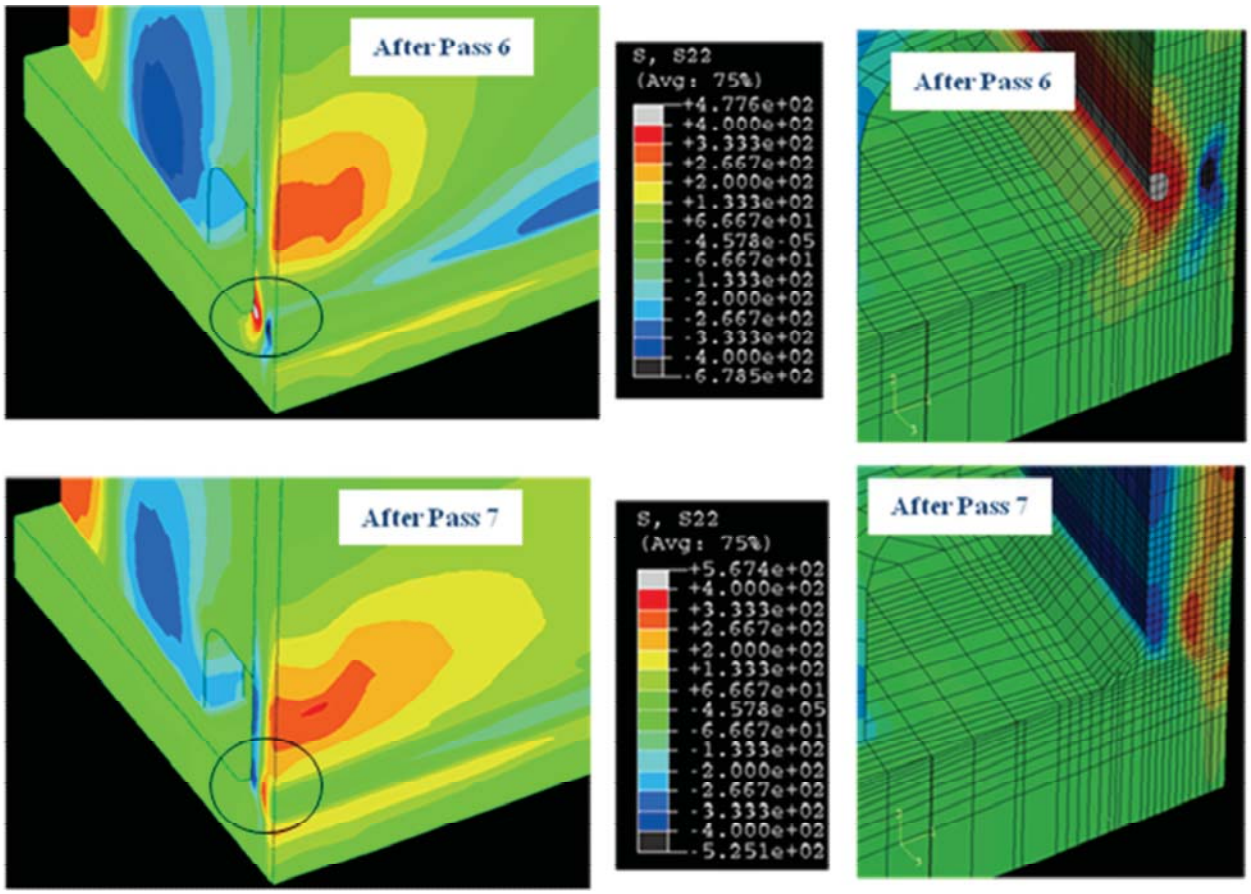

Figure 35. Axial weld residual stresses for 7-pass weld with final pass on OD. Results shown after pass 6 and pass 7.

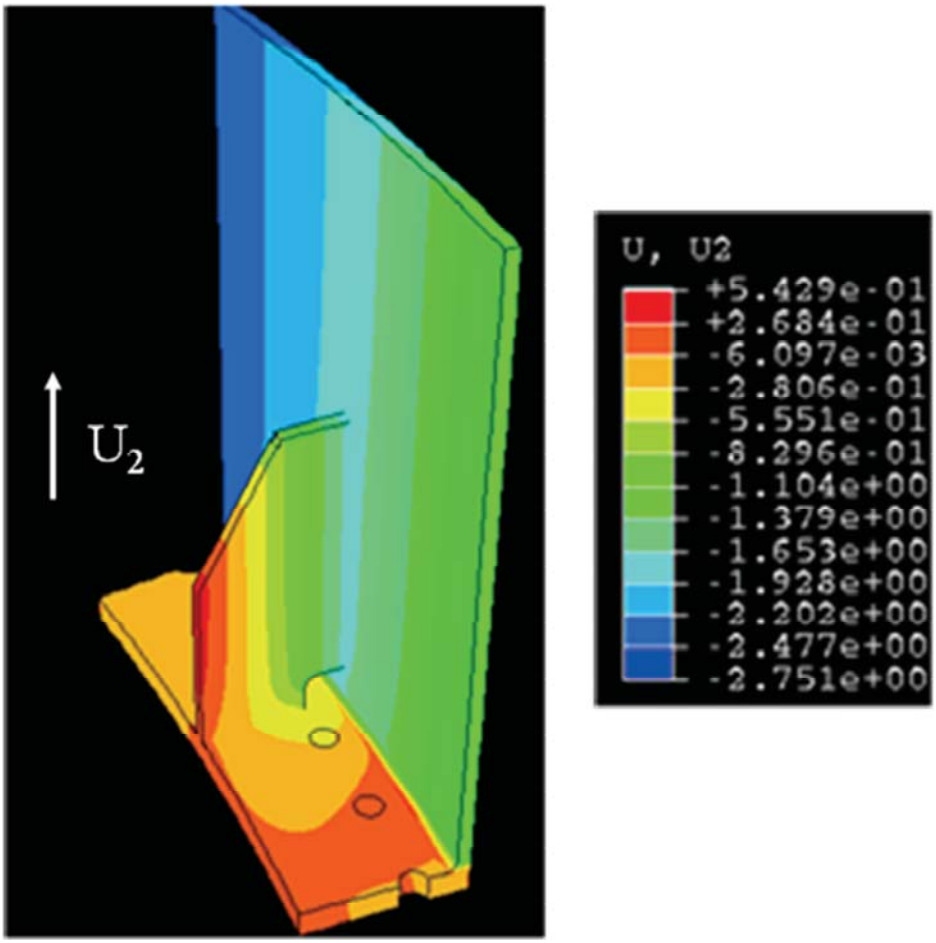

Figure 36. Vertical (U2) displacement in Ares I-X segment.

REPORT DOCUMENTATION PAGE

Form Approved
OMB No. 0704-0188

1. REPORT DATE *(DD-MM-YYYY)*	2. REPORT TYPE	3. DATES COVERED *(From - To)*
01-08-2008	Technical Memorandum	Dec 2006 - Jan 2008

4. TITLE AND SUBTITLE

Ares I-X Upper Stage Simulator Residual Stress Analysis

5a. CONTRACT NUMBER

5b. GRANT NUMBER

5c. PROGRAM ELEMENT NUMBER

6. AUTHOR(S)

Raju, Ivatury S.; Brust, Frederick W.; Phillips, Dawn R.; Cheston, Derrick

5d. PROJECT NUMBER

5e. TASK NUMBER

5f. WORK UNIT NUMBER

510505.03.0701.11

7. PERFORMING ORGANIZATION NAME(S) AND ADDRESS(ES)

NASA Engineering and Safety Center
Langley Research Center
Hampton, VA 23681-2199

8. PERFORMING ORGANIZATION REPORT NUMBER

L-19513 NESC-RP-08-09/06-081-E

9. SPONSORING/MONITORING AGENCY NAME(S) AND ADDRESS(ES)

National Aeronautics and Space Administration
Washington, DC 20546-0001

10. SPONSORING/MONITOR'S ACRONYM(S)

NASA

11. SPONSORING/MONITORING REPORT NUMBER

NASA/TM-2008-215339

12. DISTRIBUTION/AVAILABILITY STATEMENT

Unclassified-Unlimited/Publicly Available
Subject Category 39 Structural Mechanics

13. SUPPLEMENTARY NOTES

14. ABSTRACT

The structural analyses described in the present report were performed in support of the NASA Engineering and Safety Center (NESC) Critical Initial Flaw Size (CIFS) assessment for the Ares I-X Upper Stage Simulator (USS) common shell segment. An independent assessment was conducted to determine the critical initial flaw size (CIFS) for the flange-to-skin weld in the Ares I-X Upper Stage Simulator (USS). The Ares system of space launch vehicles is the US National Aeronautics and Space Administration's plan for replacement of the aging space shuttle. The new Ares space launch system is somewhat of a combination of the space shuttle system and the Saturn launch vehicles used prior to the shuttle. Here, a series of weld analyses are performed to determine the residual stresses in a critical region of the USS. Weld residual stresses both increase constraint and mean stress thereby having an important effect on fatigue and fracture life. The results of this effort served as one of the critical load inputs required to perform a CIFS assessment of the same segment.

15. SUBJECT TERMS

NESC, Critical Initial Flaw Size (CIFS), Ares I-X, upper stage stimulator, weld residual stresses, flange-to-skin

16. SECURITY CLASSIFICATION OF:			17. LIMITATION OF ABSTRACT	18. NUMBER OF PAGES	19a. NAME OF RESPONSIBLE PERSON
a. REPORT	b. ABSTRACT	c. THIS PAGE			STI Help Desk (email: help@sti.nasa.gov)
UU	UU	UU	UU	58	19b. TELEPHONE NUMBER *(Include area code)* (301) 621-0390